NAVAL POSTGRADUATE SCHOOL
Monterey, California

THESIS

B72636

Analysis of Thermospheric Dayglow Spectra from the Spacelab 1 Shuttle Mission

by

James Lee Bosserman

December 1989

Thesis Advisor: David D. Cleary

Approved for public release; distribution is unlimited.

T247172

UNCLASSIFIED
JRITY CLASSIFICATION OF THIS PAGE

REPORT DOCUMENTATION PAGE

REPORT SECURITY CLASSIFICATION UNCLASSIFIED	1b RESTRICTIVE MARKINGS
SECURITY CLASSIFICATION AUTHORITY	3 DISTRIBUTION/AVAILABILITY OF REPORT Approved for public release; distribution is unlimited.
DECLASSIFICATION/DOWNGRADING SCHEDULE	
ERFORMING ORGANIZATION REPORT NUMBER(S)	5 MONITORING ORGANIZATION REPORT NUMBER(S)

NAME OF PERFORMING ORGANIZATION Naval Postgraduate School	6b OFFICE SYMBOL *(If applicable)* 33	7a NAME OF MONITORING ORGANIZATION Naval Postgraduate School
ADDRESS *(City, State, and ZIP Code)* Monterey, CA 93943–5000		7b. ADDRESS *(City, State, and ZIP Code)* Monterey, CA 93943–5000
NAME OF FUNDING/SPONSORING ORGANIZATION	8b. OFFICE SYMBOL *(If applicable)*	9. PROCUREMENT INSTRUMENT IDENTIFICATION NUMBER

ADDRESS *(City, State, and ZIP Code)*	10 SOURCE OF FUNDING NUMBERS			
	PROGRAM ELEMENT NO.	PROJECT NO	TASK NO	WORK UNIT ACCESSION NO.

TITLE *(Include Security Classification)*
ANALYSIS OF THERMOSPHERIC DAYGLOW SPECTRA FROM THE SPACELAB 1 SHUTTLE MISSION

PERSONAL AUTHOR(S) Bosserman, James, L.

. TYPE OF REPORT Master's Thesis	13b TIME COVERED FROM ________ TO ________	14 DATE OF REPORT *(Year, Month, Day)* December 1989	15 PAGE COUNT 83

SUPPLEMENTARY NOTATION The views expressed in this thesis are those of the author and do not reflect the official policy or position of the Department of Defense or the U.S. Government

COSATI CODES			18. SUBJECT TERMS *(Continue on reverse if necessary and identify by block number)*
FIELD	GROUP	SUB-GROUP	Nitric Oxide; Thermosphere; Spacelab 1; Molecular Spectroscopy; Frank–Condon; Honl–London

ABSTRACT *(Continue on reverse if necessary and identify by block number)*

Lower thermospheric airglow spectra in the wavelength range of 1840 Å to 2280 Å were analyzed. These data were obtained by the Spacelab 1 shuttle mission in November, 1983. The analysis of the seven spectra was accomplished by comparison of the data with synthetically calculated spectra for the gamma, delta, and epsilon band emissions of nitric oxide. The tangent ray heights of the measured spectra varied in two kilometer increments from 96 km to 108 km. The strengths of 31 of the most prominent γ, δ, and ϵ band emissions were independently adjusted to achieve the best fits to the data. All of the major features in the data were identified and gave conclusive evidence of the existence of ϵ band emissions. By fitting the double bandhead feature of the emissions, the atmospheric temperature was determined for the first time from the NO emissions and compared with the temperature profile predicted by the MSIS–83 model. The

DISTRIBUTION/AVAILABILITY OF ABSTRACT ☐ UNCLASSIFIED/UNLIMITED ☒ SAME AS RPT ☐ DTIC USERS	21. ABSTRACT SECURITY CLASSIFICATION UNCLASSIFIED	
a. NAME OF RESPONSIBLE INDIVIDUAL David D. Cleary	22b TELEPHONE *(Include Area Code)* (408) 646–2828	22c. OFFICE SYMBOL 61–Cl

D FORM 1473, 84 MAR 83 APR edition may be used until exhausted. All other editions are obsolete

SECURITY CLASSIFICATION OF THIS PAGE

☆ U.S. Government Printing Office: 1986—606-243

UNCLASSIFIED

[19] Continued:

Frank–Condon factors for the v'' progression (v'=0) of the nitric oxide ϵ band were measured from the data and compared with theoretical calculations. The fluorescence efficiency of the δ bands was determined to be 0.32 ± 0.05 by fitting the δ (0,1) emission feature. Finally, a discrepancy between the observed and calculated relative intensities of the two sub–bands for the γ and ϵ bands was found.

Approved for public release; distribution is unlimited.

Analysis of Thermospheric Dayglow Spectra from the Spacelab 1 Shuttle Mission

by

James Lee Bosserman
Lieutenant, United States Navy
B.S., University of Idaho, 1983

Submitted in partial fulfillment of the
requirements for the degree of

MASTER OF SCIENCE IN PHYSICS

from the

NAVAL POSTGRADUATE SCHOOL
December, 1989

C /

ABSTRACT

Lower thermospheric airglow spectra in the wavelength range of 1840 Å to 2280 Å were analyzed. These data were obtained by the Spacelab 1 shuttle mission in November, 1983. The analysis of the seven spectra was accomplished by comparison of the data with synthetically calculated spectra for the gamma, delta, and epsilon band emissions of nitric oxide. The tangent ray heights of the measured spectra varied in two kilometer increments from 96 km to 108 km. The strengths of 31 of the most prominent γ, δ, and ϵ band emissions were independently adjusted to achieve the best fits to the data. All of the major features in the data were identified and gave conclusive evidence of the existence of ϵ band emissions. By fitting the double bandhead feature of the emissions, the atmospheric temperature was determined for the first time from the NO emissions and compared with the temperature profile predicted by the MSIS–83 model. The Frank–Condon factors for the v'' progression ($v'=0$) of the nitric oxide ϵ band were measured from the data and compared with theoretical calculations. The fluorescence efficiency of the δ bands was determined to be 0.32 ± 0.05 by fitting the δ (0,1) emission feature. Finally, a discrepancy between the observed and calculated relative intensities of the two sub–bands for the γ and ϵ bands was found.

TABLE OF CONTENTS

I. INTRODUCTION 1
  A. THESIS OBJECTIVES 1
  B. THESIS OUTLINE 2
II. THE NEUTRAL ATMOSPHERE 3
  A. BACKGROUND 3
  B. NITRIC OXIDE CHEMISTRY IN THE LOWER THERMOSPHERE 4
III. THE SYNTHETIC SPECTRA MODEL 8
  A. INTRODUCTION 8
  B. DIATOMIC MOLECULAR SPECTROSCOPY 8
  C. THE SYNTHETIC SPECTRA 17
    1. Line Positions 17
    2. Molecular State Populations 24
    3. Selection Rules and Transition Probabilities 30
    4. Synthetic Spectra Calculations 35
IV. THE SPACELAB 1 SHUTTLE MISSION 37
  A. INTRODUCTION 37
  B. THE INSTRUMENT 37
  C. OVERVIEW 41
    1. Flight Parameters for Low Altitude Viewing 41
    2. The Space Shuttle Optical Environment 43
  D. THE OBSERVED SPECTRA 44

V. DATA ANALYSIS 47
  A. INTRODUCTION 47
  B. APPLICATION OF THE SYNTHETIC SPECTRA 47
  C. FITTING THE DATA 52
  D. TEMPERATURE COMPARISON 62
  E. MEASURED FRANK–CONDON FACTORS FOR THE EPSILON BAND 64
  F. ADDITIONAL FEATURES OF THE SPECTRA 65
    1. Relative Sub–band Intensities 65
    2. NO Delta Bands 67
VI. CONCLUSION 69
  A. SUMMARY OF FINDINGS 69
  B. TOPICS FOR FURTHER INVESTIGATION 70
BIBLIOGRAPHY 71
INITIAL DISTRIBUTION LIST 74

LIST OF FIGURES

FIGURE PAGE

2–1 Odd Nitrogen Production/Loss Mechanisms....6

3–1 Electronic, Vibrational, and Rotational Levels....12

3–2 Vibration–Rotation Band Structure....13

3–3 Potential Energy Diagram for NO....16

3–4 Vector Diagrams for Hund's Coupling Cases....22

3–5 Λ–Type Doubling in the $^2\Pi$ State....23

3–6 Term Diagram for NO Gamma Band Transitions....32

3–7 Term Diagram for $^2\Pi \rightarrow {}^2\Pi$ Transitions....33

3–8 Synthetic Spectra for (1,0) Gamma Band Emissions....36

4–1 Optical Design of Spectrometer....39

4–2 Roll Method for Low Altitude Scanning....41

4–3 Spatial Imaging Method for Low Altitude Viewing....42

4–4 Measured Spectra....46

5–1 Calculated NO Synthetic Spectra....50

5–2 Representative Convolved Synthetic Spectrum....51

5–3 Comparison of Synthetic Spectra With and Without Higher Altitude Contributions....52

5–4 Comparison of Data and Synthetic Fit at 96 km....53

5–5 Comparison of Data and Synthetic Fit at 98 km....54

5–6 Comparison of Data and Synthetic Fit at 100 km....55

5–7 Comparison of Data and Synthetic Fit at 102 km....................................56
5–8 Comparison of Data and Synthetic Fit at 104 km....................................57
5–9 Comparison of Data and Synthetic Fit at 106 km....................................58
5–10 Comparison of Data and Synthetic Fit at 108 km....................................59
5–11 NO Column Density..61
5–12 Effects of Temperature Variations on the Fit...63
5–13 Temperature Comparison...64
5–14 v" Progression for v'=0 in Epsilon Band..66
5–15 Frank–Condon Factor Comparison...66
5–16 Synthetic Fit Without Honl–London Factor Increase...............................68

I. INTRODUCTION

Lower thermospheric airglow spectra obtained by the Spacelab 1 shuttle mission in the wavelength range of 1840 to 2280 angstroms are presented and analyzed. The emission bands of nitric oxide dominate this portion of the ultraviolet spectrum and therefore the data are analyzed by comparison with synthetic spectra for the nitric oxide emissions. The relative intensities of the various emissions are analyzed as a function of altitude over the range of 96 to 108 kilometers. Additionally, NO delta band fluorescence efficiency, effects of variations in temperature, contributions to the spectra by constituents other than nitric oxide, and the pertinent photochemical reactions at the altitudes of interest are investigated. The technique of modeling the data with synthetic spectra allows for an investigation of thermospheric processes as well as providing corrections, modifications, and updates to the model of the synthetic spectra.

A. THESIS OBJECTIVES

This work focuses on seven spectra obtained by the Spacelab 1 shuttle mission. Each observed spectrum is modeled by a calculated synthetic spectrum in which the relative strengths of 31 of the most prominent gamma, delta, and epsilon band transitions of nitric oxide can be independently adjusted. Small contributions by the Vegard–Kaplan bands and the Lyman–Birge–Hopfield (LBH) band system of molecular nitrogen are also included in the fit. Causes for the variations in the strengths of the major transitions as a function of altitude are presented and several other notable spectral features are discussed.

B. THESIS OUTLINE

This thesis is divided into six chapters. Chapter II gives some general background information on the neutral atmosphere with its various regions and properties, and discusses the fundamentals of nitric oxide chemistry in the lower thermosphere.

In Chapter III the synthetic spectra model is developed and discussed in depth. This is accomplished by reviewing diatomic molecular spectroscopy to include line positions, molecular state populations, selection rules, and transition probabilities. These topics are then combined to calculate the synthetic spectra.

Chapter IV gives the background on the Spacelab 1 shuttle mission and the instrumentation used in obtaining the measured spectra. The actual data are also presented in this chapter.

In Chapter V the data are analyzed. Each measured spectrum is fit as closely as possible to the synthetic spectra. Factors contributing to the variations in intensities of the major emissions as a function of altitude are discussed.

Chapter VI concludes the paper with a summary of the findings and some suggestions for additional investigations.

II. THE NEUTRAL ATMOSPHERE

A. BACKGROUND

The Earth's atmosphere is a highly dynamic medium. Convective mixing, differential heating due to solar radiation, and the planet's rotation combine to produce a partial stratification of the atmosphere. This layering effect is usually described two ways. The first is by temperature profile and the second is by chemical composition. In the first instance, the lowest ten kilometers of the atmosphere is known as the *troposphere* and in this region the temperature steadily decreases from about 300 K at the surface to around 220 K at ten kilometers. At this point the temperature profile passes through an isothermal region and then begins to increase with altitude up to a height of around 45 kilometers. This second region is called the *stratosphere.* Above the stratosphere the temperature again begins to decrease with increasing altitude to a low of about 180 K around 85 kilometers in the region labeled the *mesosphere.* Above the mesosphere the temperature increases rapidly with increasing altitude until an isothermal equilibrium is reached, usually between 300–500 kilometers, depending upon the level of solar activity. This region is known as the *thermosphere* and it has no sharply defined upper limit. The temperatures at the upper equilibrium point may reach as high as 2000 K (kinetic temperature) during peak levels of solar activity.

The second method of labelling is dictated by the interactions of the atoms and molecules in the atmosphere. In this scheme the lower 100 kilometers of the atmosphere is denoted as the *homosphere* because the vertical mixing of all species of atoms and molecules keeps their relative densities roughly constant over the entire region. Above 100 kilometers the densities of the various constituents become low enough that the "mixing" action diminishes rapidly with increasing altitude. Thus, each particular species is free to reach hydrostatic equilibrium separately and its density profile follows its own separate scale height. This region is the *heterosphere* and extends out to about 500 kilometers. The *exosphere*, or "outer atmosphere," extends beyond the heterosphere, with again no clearly defined upper limit, and is a region of extremely low densities and high kinetic temperatures.

This paper focuses on the lower thermosphere (also lower heterosphere) where there is a strong positive temperature gradient and where convective mixing of the molecules is no longer a major concern.

B. NITRIC OXIDE CHEMISTRY IN THE LOWER THERMOSPHERE

Nitric oxide (NO) is one of several "trace constituents" in the atmosphere. Although the density of NO in the lower thermosphere may be several orders of magnitude smaller than the abundant species (i.e. molecular and atomic oxygen and molecular nitrogen), its presence is important. It was noted (Crutzen, 1971) that NO can act as a catalyst in the destruction of ozone (O_3) and as such, the small amount of NO is preserved while large amounts of ozone may be destroyed. The catalytic processes are given in the following reactions:

$$NO + O_3 \rightarrow NO_2 + O_2 \qquad (2\text{–}1)$$

and

$$NO_2 + O \rightarrow NO + O_2 \qquad (2\text{–}2)$$

which equate to a net reaction of:

$$O_3 + O \rightarrow 2O_2. \qquad (2\text{–}3)$$

It is clear from the above reactions that the amount of NO remains constant while serving to reduce the amount of ozone. At very high latitudes the normal daytime photodissociation of the molecules may be severely restricted due to the shortness of the daylight hours and exceptionally long nights. Under these circumstances the molecules may have long enough lifetimes to be transported down to stratospheric heights (Strobel et.al., 1970; Barth, 1984). Thus, stratospheric ozone levels may be affected by this process.

Another significant aspect of nitric oxide is its low first ionization potential of 9.25 eV. This makes NO the only major atmospheric constituent that can be ionized by the strong Lyman–α emission from the sun at 1216 Å. It is this ionization of NO that is responsible for the formation of the D–region of the ionosphere.

Nitric oxide is the most abundant form of the "odd nitrogen" family which is comprised of all photochemically active, nitrogen–containing species. Other forms include $N(^4S)$, $N(^2D)$,and $N(^2P)$, (the ground state, first, and second excited states of atomic nitrogen) and NO_2. The production and loss mechanisms will not be investigated in depth here as they are not the thrust of this paper. However, the various chemical reactions, their associated reaction rates, and sources were tabulated by Cleary (1986). Figure 2–1 is a schematic representation of these reactions for the odd nitrogen species in the thermosphere. The figure shows that as photons or high energy electrons interact with the major atmospheric

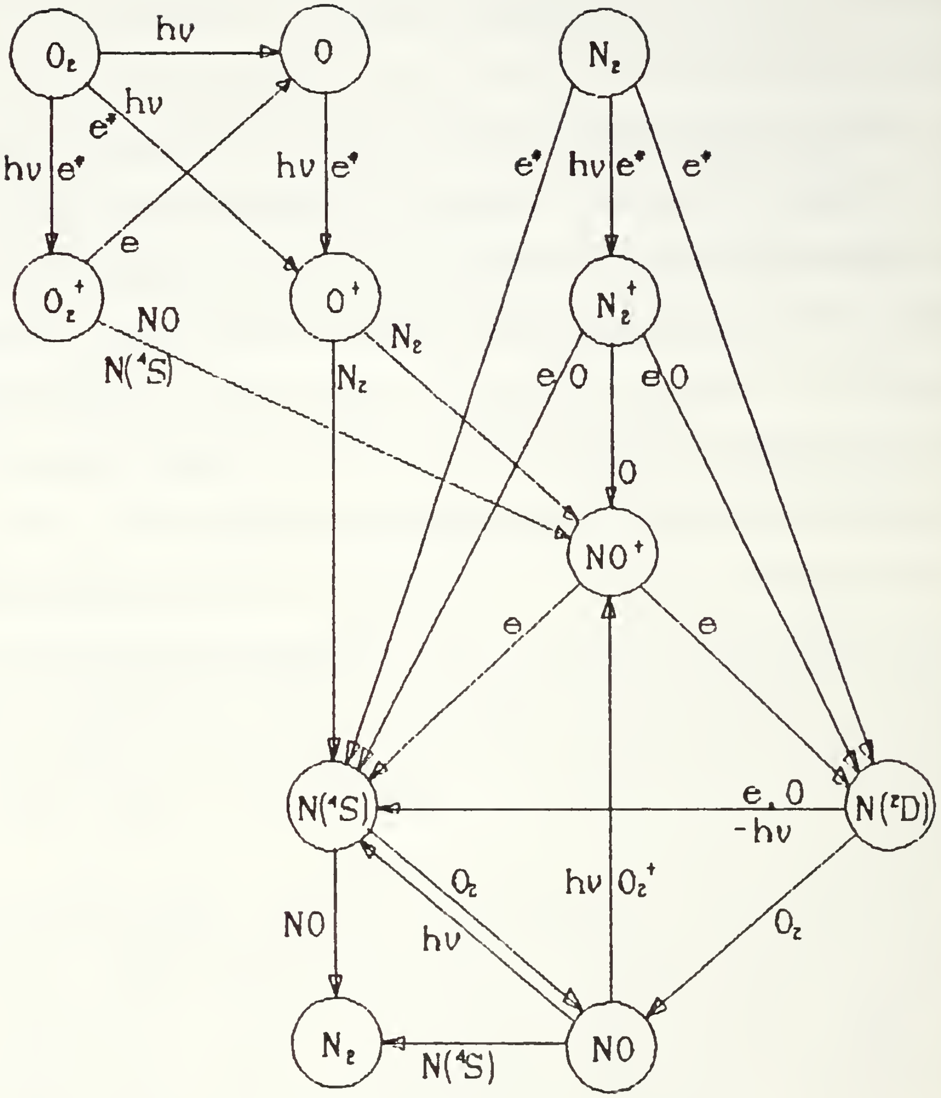

Figure 2–1 Odd Nitrogen Production/Loss Mechanisms

constituents of O, O_2, and N_2 their respective ions are formed. As these ions interact with the other atmospheric constituents, many ultimately terminate as NO^+. The NO^+ ion, with its low ionization potential, is known as the "terminal ion" in the ionosphere. The only major loss mechanism for the NO^+ ion is dissociative recombination which produces either $N(^2D)$ and O or $N(^4S)$ and O.

Although the development of a photochemical model will not be pursued in this paper, the use of MSIS–83 (Hedin, 1983) which computes the neutral atmosphere and temperature profile between 86 and 450 kilometers will be used as a tool during the data analysis in Chapter V. The temperature profile is known to show a strong positive gradient in the region of interest in this paper. The temperatures that are predicted by the MSIS–83 model will be compared with those that are determined from fitting the synthetically calculated spectra to the data.

III. THE SYNTHETIC SPECTRA MODEL

A. INTRODUCTION

Through spectroscopic analysis the chemical compositions of materials, the air, and nearly any other object of interest can be determined. The spectral emission (or absorption) features are nature's own "fingerprints" for any particular substance. More specifically, the study of the atmospheric dayglow provides a means to "map" the atmosphere as functions of chemical composition, temperature, altitude, and reaction processes. From a military standpoint, a more thorough understanding of the upper atmosphere could lead to major improvements in systems such as the over–the–horizon radars.

An extremely useful analysis technique in molecular spectroscopy is the comparison of synthetically (theoretically) produced spectra with actual measured spectra. The synthetic spectra can be used to show predicted spectral features as well as rule out specific molecular transitions as causes for unknown features. In this chapter the calculation of the synthetic spectra for nitric oxide is presented, and these spectra will later be used in the analysis of the Spacelab 1 data. A brief review of diatomic molecular spectroscopy begins the discussion, and the actual calculation of the synthetic spectra follows.

B. DIATOMIC MOLECULAR SPECTROSCOPY

An in–depth understanding of molecular spectroscopy is essential if one is to calculate the synthetic spectra. There are many texts and references available that discuss molecular spectroscopy. For a very thorough treatment of the subject, Spectra of Diatomic Molecules by Gerhard Herzberg (1950) is recommended. It is from this reference that the majority of the following discussion is taken.

The simplest model for a diatomic molecule is that which considers the molecule as a dumbbell with the two atoms, masses m_1 and m_2, connected by a massless, rigid rod of length *r*. In reality, the atoms are not separated at a fixed distance but the separation distance varies as the molecule undergoes motion. The two possible motions for the atoms are 1) rotation about the center of mass of the two–atom system, and 2) vibrational motion of the atoms toward and away from each other. It has been shown through quantum mechanics that the parameters that describe these motions may not take on arbitrary values but rather are quantized. That is, the molecule may only rotate at specific, discrete speeds and vibrate with specific, discrete frequencies.

In the rotational case, application of the Schrödinger equation leads to discrete energy levels, E, such that:

$$E(J) = \frac{h^2 J(J+1)}{8\pi^2 \mu r^2} , \qquad (3\text{–}1)$$

where h is Planck's constant, J is the rotational quantum number (J = 0,1,2,...), and μ is the reduced mass of the two–atom system. Now, μr^2 is the moment of inertia, I, for rotation of the dumbbell so the rotational energies of the molecule are inversely proportional to the moment of inertia. The rotational *term value* is the rotational energy divided by hc and is denoted in the literature by F(J). So the rotational term value can be written as:

$$F(J) = \frac{E}{hc} = BJ(J+1) \ , \tag{3–2}$$

where $B = h/8\pi^2 cI$ is called the *rotational constant* of the molecule.

For the vibrational motion, the molecule is classically represented by the two atoms being connected by a spring instead of a rigid rod. Once disturbed, the atoms would respond in simple harmonic motion about the center of mass of the system. Solutions to the Schrödinger equation for the simple harmonic oscillator problem are well known given that the potential energy curve for such a system is parabolic. Recalling that quantum mechanics will allow only discrete values for the vibrational energies, these energies are then given by:

$$E(v) = \frac{h}{2\pi}\sqrt{\frac{k}{\mu}}\,(v + \tfrac{1}{2}) \ , \tag{3–3}$$

where v is the vibrational quantum number, μ is the reduced mass, and k is the force constant for the atomic interaction. As in the rotational case, we can define the vibrational term value as the vibrational energy divided by hc. Then the vibrational term value can be written:

$$G(v) = \frac{E(v)}{hc} = \omega(v + \tfrac{1}{2}) \ , \tag{3–4}$$

where ω is a constant of the molecule.

These expressions for the rotational and vibrational term values are approximations as neither the non–rigid rotator nor the anharmonicity of the simple harmonic oscillator were taken into account. However, for now let the term value for the vibration and rotation of a molecule be given by $T = G(v) + F(J)$.

The rotational, vibrational, and electronic states of a molecule combine in a nested manner. Within a given electronic energy state there are many vibrational energy levels. Similarly, within each vibrational energy level there are many rotational energy levels. Figure 3–1 schematically represents these relationships between the electronic, vibrational, and rotational energy levels.

In the case of purely rotational transitions within a given vibrational and electronic state, the allowed transitions for electric dipole radiation restrict the change in rotational quantum number, J, to $\Delta J = \pm 1$. Typical energies of these transitions are 10^{-4} to 10^{-3} eV which is quite low. For example, at room temperature the thermal energy of the molecules is about 0.025 eV so ordinary collisions of molecules can excite the molecules to higher rotational energies.

Transitions between the rotational levels of two different vibrational levels produce what is known as vibration–rotation spectra. The selection rule governing these transitions is also $\Delta J = \pm 1$. In molecular spectroscopy, superscripts of primes are used to designate the upper and lower states of a transition. A single prime denotes the upper state and a double prime denotes the lower state. Remembering the selection rule that $\Delta J = \pm 1$, a molecule in the $J' = 4$ state can make a transition to the $J'' = 5$ or $J'' = 3$ state. All of the transitions in which $\Delta J = +1$ are referred to as R–branch transitions and those with $\Delta J = -1$ are called P–branch transitions. The ΔJ is the difference in the

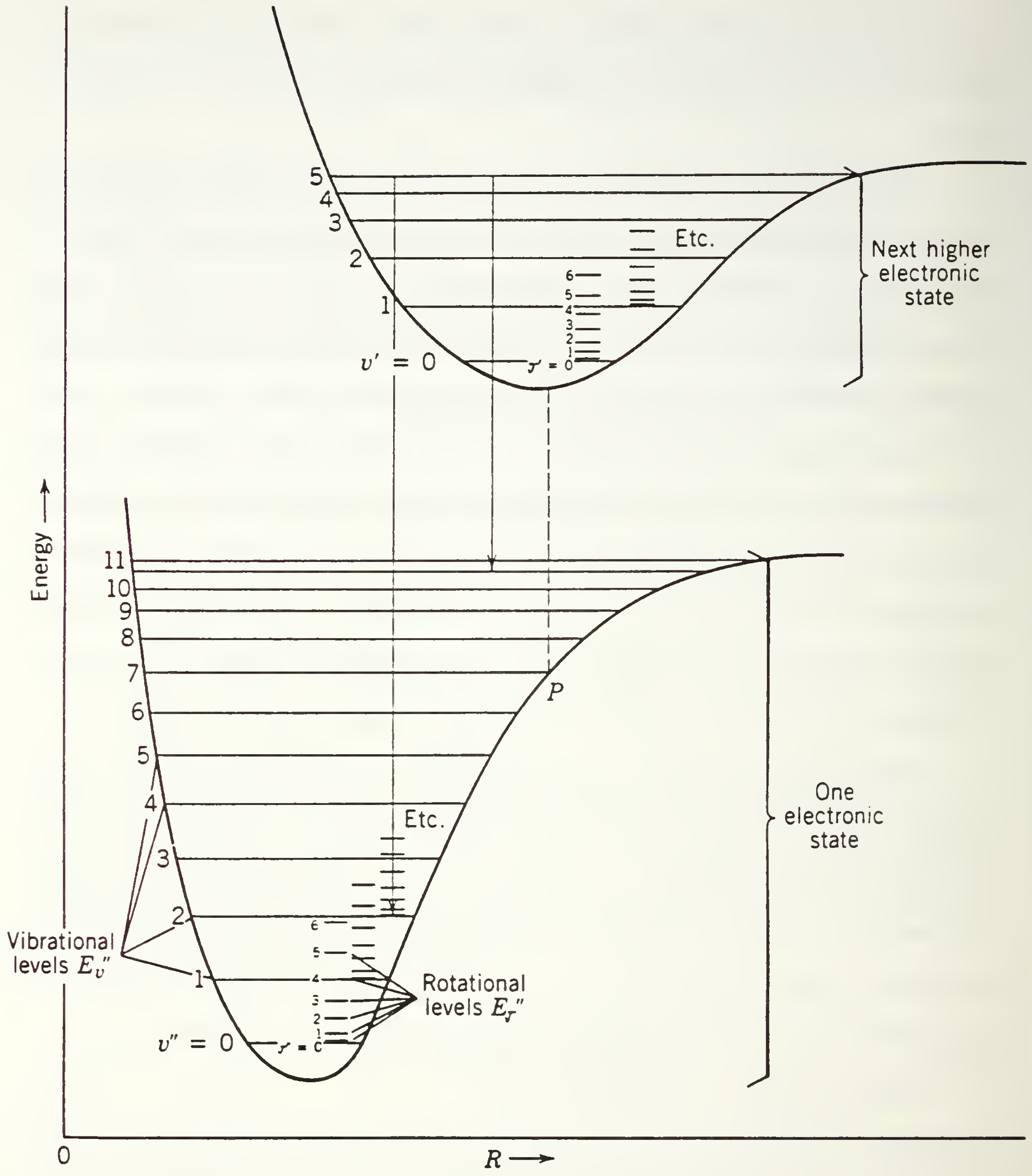

Figure 3–1 Electronic, Vibrational, and Rotational Levels

(from Eisberg and Resnick, 1985)

rotational quantum number between the upper and lower states, i.e., ΔJ = J' − J". The combination of the two branches forms a vibration–rotation band. Figure 3–2 shows the notation for such a band.

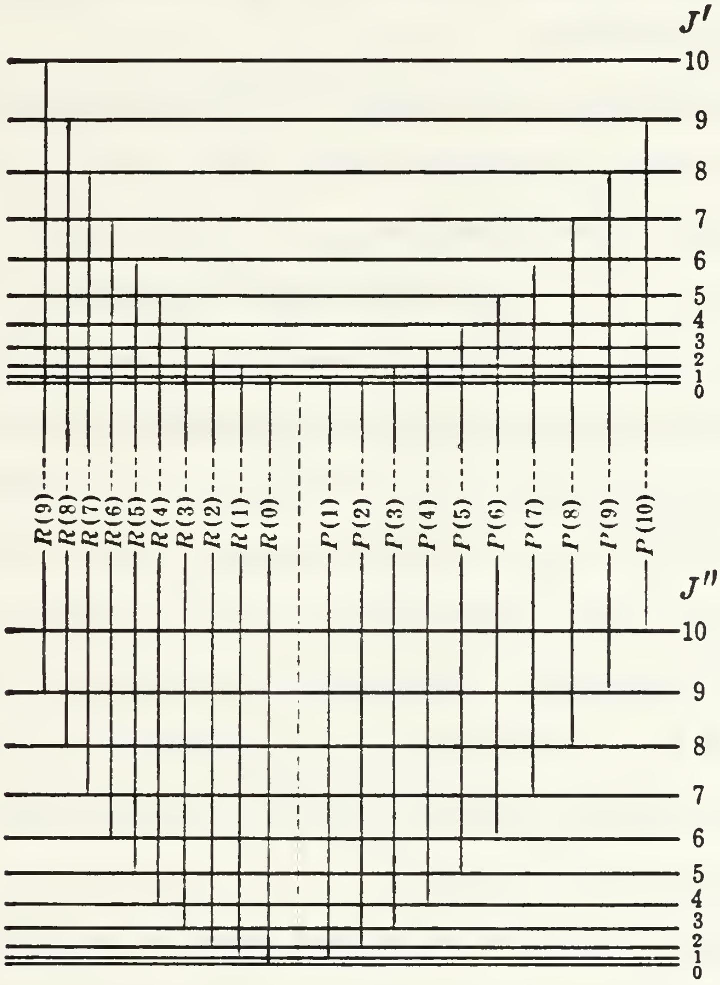

Figure 3–2 Vibration–Rotation Band Structure

(from Herzberg, 1950)

In a similar manner in which the purely rotational transitions were extended to include vibrational transitions, the vibrational–rotational transitions can be extended to include transitions between different electronic energy levels. Therefore, the electronic state of the molecule also needs to be addressed. Just as in individual atoms, the orbital configuration of the electrons around the molecule determine its electronic energy.

Diatomic molecules are a special case of molecules in that their electrostatic field is symmetric along the internuclear axis. Again, as in the case of atomic systems, the orbital angular momentum of the electrons around the molecule combine vectorially to form a total orbital angular momentum, L. This orbital angular momentum vector in general will be directed at some angle away from the internuclear axis and will precess around the internuclear axis. Because of this precession, the orbital angular momentum itself is not a good quantum number. However, the component of L along the internuclear axis is a constant of the motion and as such makes a good quantum number by which to classify the electronic states of the molecule. This component of L can be denoted M_L and can take on values $M_L = L, L-1, L-2, \ldots, -L$. The magnitude of the component of the orbital angular momentum along the internuclear axis is given its own symbol, Λ. So $\Lambda \equiv |M_L|$ and then $\Lambda = 0,1,2,\ldots L$.

The designations for the various quantum values for the molecules are quite analogous to those for atomic state designations. For example, in atomic states the values for the orbital angular momentum, L, are given by S,P,D,... for L = 0,1,2,... respectively. Similarly, in molecular states the Roman letters are replaced by Greek letters such that $\Sigma, \Pi, \Delta, \ldots$ correspond to Λ values of 0,1,2,... respectively.

The spin angular momentum of the electrons orbiting the molecule will combine to form a resultant spin, S. In Σ states, this resultant spin vector is not affected by an internal magnetic field and hence will not precess about the internuclear axis unless an external magnetic field is present. In the cases where $\Lambda \neq 0$, the orbiting electrons set up an internal magnetic field in the molecule causing S to precess about the internuclear axis. The component of S that lies along the internuclear axis, M_S, is a constant of the motion and becomes useful as a quantum number. This component of the spin is denoted by Σ and can take on the values $\Sigma = S, S-1, S-2, \ldots, -S$. Thus, there are $2S + 1$ possible values which give rise to the multiplicity of the particular state.

As previously mentioned during the discussion of orbital angular momentum. there are strong similarities between the molecular state spectroscopic notation and that of the atomic notation. As in the atomic spectroscopic case, the multiplicity of a given molecular state is written as a left superscript. Additionally, for molecular states in which Σ is non–zero, the value $(\Lambda + \Sigma)$ may be written as a right subscript. For example, the ground state of NO is a $^2\Pi$ state which is split into the $^2\Pi_{3/2}$ and $^2\Pi_{1/2}$ states.

For a given molecule, the various electronic states are also given letter designations for convenience. The letter designations may be either upper case or lower case depending on multiplicity factors. The ground state of a molecule is generally given an X designation. The first, second, and other higher energy excited states with the same multiplicity as the ground state are labelled with A,B,C,... and so forth. The multiplicity of a state may differ from that of the ground state by 2 depending upon the allowed spin configurations. The higher energy excited states that differ in multiplicity from the ground state are labelled with lower case letters instead of capital letters. Figure 3–1 shows the generic relationships of the electronic, vibrational, and rotational energy levels. In Figure 3–3 the potential energy diagram for nitric oxide is shown utilizing the aforementioned labelling scheme.

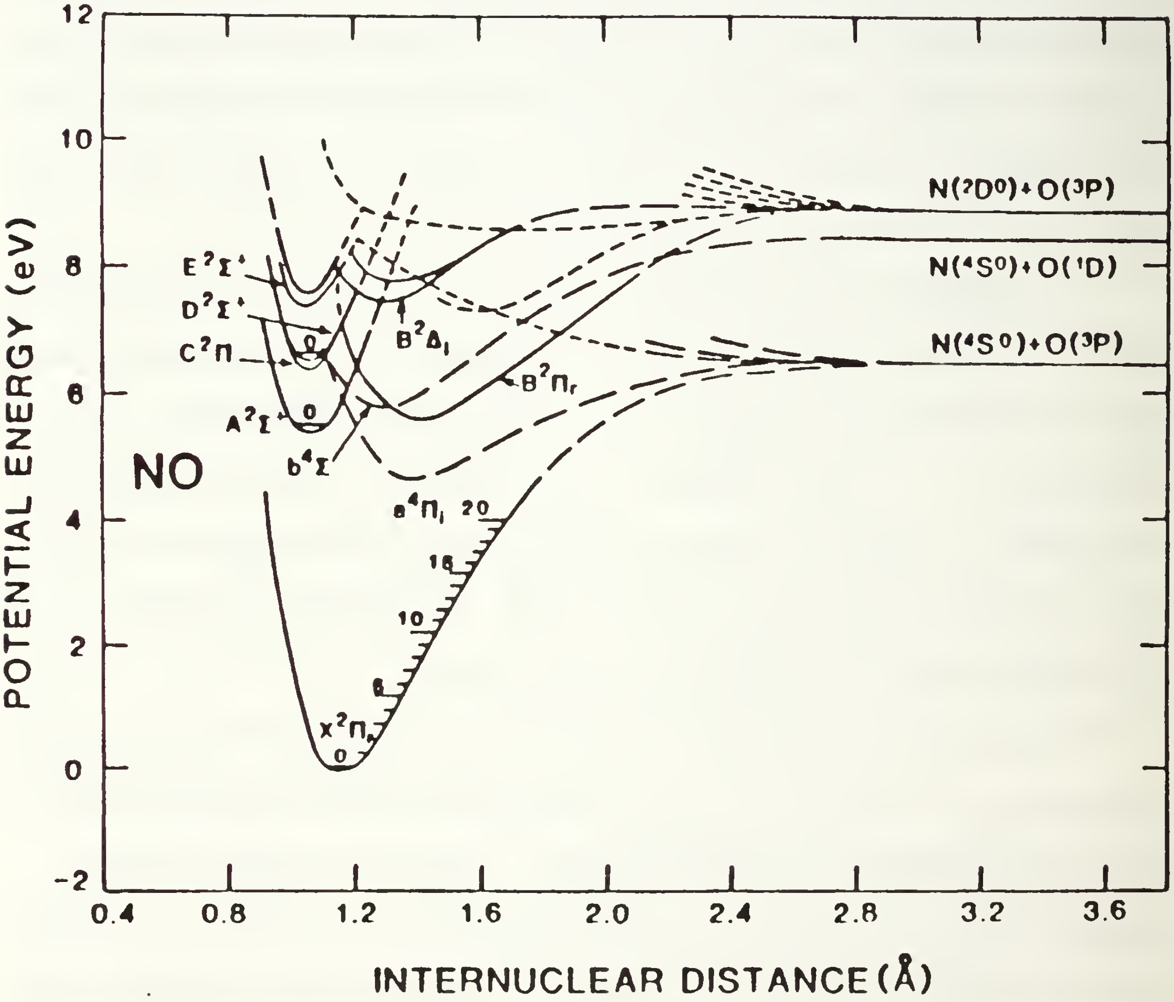

Figure 3–3 Potential Energy Diagram for NO (from Gilmore, 1965)

One last labelling scheme will be mentioned before the discussion of the actual calculation of the synthetic spectra begins. This labelling group describes transitions between electronic states. For example, all transitions between the first excited state of NO and the ground state ($A^2\Sigma \rightarrow X^2\Pi$) are designated as *gamma band* transitions. Similarly, the *delta band* transitions involve those transitions between the $C^2\Pi$ and $X^2\Pi$ states and the *epsilon band* transitions are those between the $D^2\Sigma$ and $X^2\Pi$ states. The gamma, delta, and epsilon bands of nitric oxide will be explored in depth in this paper and it is these bands that will be calculated synthetically.

C. THE SYNTHETIC SPECTRA

1. Line Positions

The line position, σ, or wave number (cm^{-1}) of a spectral line is 1/hc times the energy difference between the initial and final states of the transition that produced the line. When the quantum state energies of a molecule are measured relative to the ground state and are expressed in wave numbers, they are called term values. Recall that the earlier discussion for the rotational and vibrational term values were their respective energies divided by hc. Now the electronic term value is added to the rotational and vibrational term values to give:

$$T = T_e + G(v) + F(J), \tag{3-5}$$

where T_e is the electronic term value and G(v) and F(J) are as previously discussed. Thus, the line position for a transition between the states (T_e',v',J') and (T_e'', v'', J'') can be expressed as:

$$\sigma = T_e' - T_e'' + G'(v') - G''(v'') + F'(J') - F''(J''). \qquad (3\text{–}6)$$

Band systems such as the NO gamma, delta, and epsilon bands involve transitions between two specific electronic states. In such transitions, the values of T_e' and T_e'' are fixed and can be expressed as a new quantity, $\sigma_e = T_e' - T_e''$. Thus, the line positions for a particular band system can be written as:

$$\sigma = \sigma_e + G'(v') - G''(v'') + F'(J') - F''(J''). \qquad (3\text{–}7)$$

A molecular band will include all of the transitions between the vibrational levels v' and v'' and may consist of hundreds of lines due to the transitions between the numerous rotational levels. Now for a given v' and v'' the term value for each line can be written:

$$\sigma_{j'j''} = \sigma_0 + F'(J') - F''(J''), \qquad (3\text{–}8)$$

where σ_0 is called the *band origin* and is given by:

$$\sigma_0 = \sigma_e + G'(v') - G''(v''). \qquad (3\text{–}9)$$

The values for T_e used in the above calculations are determined from laboratory measurements and can be found for most diatomic molecules in a compilation by Huber and Herzberg (1979).

Looking more closely at the vibrational and rotational term values, it is necessary to use better approximations than the rigid rotator and the simple harmonic oscillator descriptions that were previously introduced. In the vibrational case, the anharmonicity of the potential energy curves shown in Figure 3–3 must be considered and in the rotational case the nonrigid rotator requires consideration.

Including the effects of anharmonicity, the vibrational term value is given by:

$$G(v) = \omega_e(v + \tfrac{1}{2}) - \omega_e x_e(v + \tfrac{1}{2})^2, \qquad (3\text{–}10)$$

where the second term on the right corrects for anharmonic effects and the values ω_e and $\omega_e x_e$ are constants of the molecule and can be found in the Huber and Herzberg compilation.

In the situation of the nonrigid rotator, the multiplicity of the state becomes a factor and separate cases need to be considered. In the case of singlet states (i.e., $S = 0$) the rotational term value is expressed as:

$$F(J) = B_v J(J + 1) - D_v J^2(J + 1)^2, \qquad (3\text{–}11)$$

where the second term on the right includes the effects of the nonrigid rotator. B_v and D_v depend on the vibrational level of the molecule and are given by:

$$B_v = B_e - \alpha_e(v + \tfrac{1}{2}) + \text{...higher order terms} \qquad (3\text{–}12)$$

and

$$D_v = D_e - \beta_e(v + \frac{1}{2}) + \text{...higher order terms} \qquad (3\text{–}13)$$

with the constants B_e, α_e, D_e, and β_e given in the compilation of diatomic molecular constants by Huber and Herzberg (1979).

In the case where the multiplicity of the molecular state is greater than one, as in the doublet states of NO which are of interest in this paper, the rotational term value is highly dependent upon the coupling between Λ and Σ. Hund (1927) used a vector model to represent the electronic and nuclear angular momenta and was able to classify five coupling schemes according to the strength of the interactions. The first two coupling schemes, Hund's case (a) and Hund's case (b), are the most common (and are applicable to the NO synthesis in this paper) and will be the only two cases discussed here.

In Hund's case (a), the motion of the electrons (both orbital and spin) is strongly coupled to the internuclear axis but at the same time is weakly coupled to the rotation of the molecule. The components of electronic angular momentum along the internuclear axis, Λ and Σ, combine to form a total electronic angular momentum vector, Ω, along the axis such that $\Omega = | \Lambda + \Sigma |$. Figure 3–4a shows the orientation of the various vector components. Ω combines with the nuclear angular momentum vector, N, to produce the resultant total molecular angular momentum vector, J.

Hund's case (b) is characterized by weak (or zero) coupling of S to the internuclear axis. The orbital part of the electronic motion is still strongly coupled to the axis but more moderately coupled to the rotational motion.

Additionally, when $\Lambda = 0$ case (a) cannot apply and the angular momentum, K, (see Figure 3–4b) is identical to N and is perpendicular to the internuclear axis. In this notation, K comprises all angular momentum components except for electron spin. The spin angular momentum vector combines with K (or N as appropriate) to form the total molecular angular momentum, J.

The amount of splitting of the energy levels of a multiplet state depends upon which of the coupling schemes the molecule most closely obeys. For the most part, the splitting for Hund's case (a) coupling is large and the splitting for Hund's case (b) coupling is negligibly small. To a good approximation then, the amount of multiplet splitting can be given by:

$$T_e = T_0 + A\Lambda\Sigma, \tag{3–14}$$

where Λ and Σ are as previously defined and A is a constant for the particular multiplet term. The constant A then will be large for Hund's case (a) and small or even zero for Hund's case (b).

The Hund's coupling cases represent idealized limiting cases. In general, a molecular state does not fit neatly into just one specific coupling scheme. These coupling cases do, however, represent the observed spectra to good approximation in many instances. For higher degrees of rotational excitation, a transition between coupling schemes is observed. There are two types of uncoupling mechanisms between the case (a) and case (b) coupling schemes. These uncoupling mechanisms are *Λ–type doubling* and *spin–type uncoupling.* Both mechanisms will cause a splitting or doubling of the energy levels.

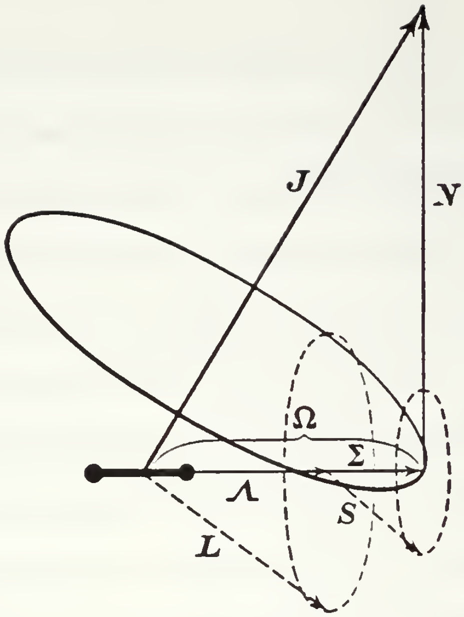

Hund's Coupling Case (a)

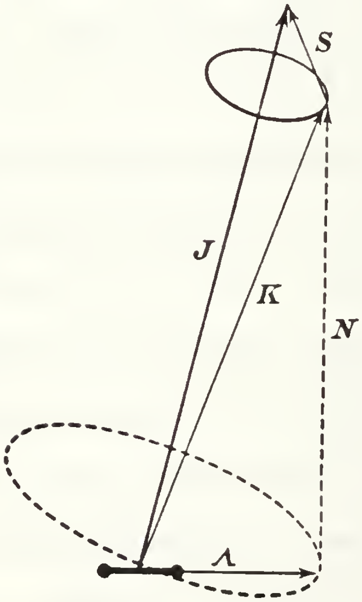

Hund's Coupling Case (b)

Figure 3–4 Vector Diagrams for Hund's Coupling Cases

(from Herzberg, 1950)

In Hund's cases (a) and (b), Λ–type doubling occurs for $\Lambda \neq 0$ states (i.e., Π,Δ,...etc.) and increases with increasing rotational speeds. For the doublet Π states of NO, the Λ–type doubling amounts to only a fraction of a cm^{-1}. Figure 3–5 illustrates this type of doubling for the doublet Π molecular states.

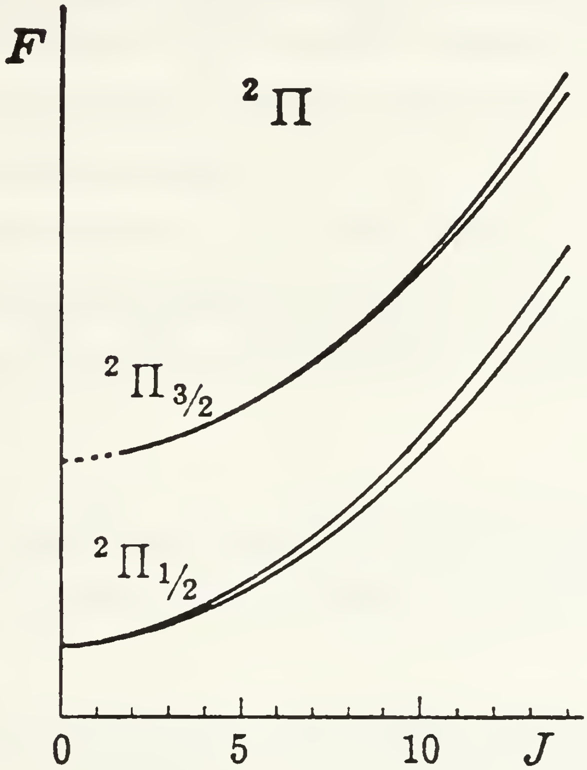

Figure 3–5 Λ–Type Doubling in the $^2\Pi$ State

(from Herzberg, 1950)

In spin uncoupling, or spin–type doubling, the spin, S, begins to uncouple from the internuclear axis as the rotational speed becomes comparable to the precession of S about L. For small rotation the coupling is strong and the splitting is large (case (a)). For large rotation the coupling is weak and the amount of splitting is drastically reduced (case (b)). The result of this larger splitting due to the spin–type uncoupling gives rise to different rotational term values for the different spin sub–states. For a doublet state, the two rotational term values are:

$$F_1(J) = B_v\left[(J + \tfrac{1}{2})^2 - \Lambda^2 - \tfrac{1}{2}\sqrt{4(J + \tfrac{1}{2})^2 + Y(Y - 4)\Lambda^2}\ \right] - D_v J^4 \tag{3–15a}$$

and

$$F_2(J) = B_v\left[(J + \tfrac{1}{2})^2 - \Lambda^2 + \tfrac{1}{2}\sqrt{4(J + \tfrac{1}{2})^2 + Y(Y - 4)\Lambda^2}\ \right] - D_v(J + 1)^4, \tag{3–15b}$$

where $Y = A/B_v$ and the subscripts of F_1 and F_2 refer to the terms $J = K + \frac{1}{2}$ and $J = K - \frac{1}{2}$ respectively. Again, K is the resulting angular momentum, neglecting spin.

The gamma, delta, and epsilon bands all involve transitions from and to doublet states, so Equations 3–15a and 3–15b will be used in the calculation of the appropriate term values. Combining these relations with those of Equations 3–5 and 3–10 the line position for all transitions can be found.

2. Molecular State Populations

To correctly calculate the population of a specific molecular state, that state must be precisely defined. Up to this point, a specific molecular state has been defined by n,v,Σ, and J for Hund's case (a) and by n,v,N, and J for Hund's case (b). As previously mentioned, states in which $\Lambda > 0$ are additionally split by the Λ–type doubling. This doubling introduces a *parity* quantum number, p, since the two components of the Λ–doublet have opposite parity (+ or –) due to $\Lambda = |M_L|$. The calculation of the line positions is not sensitive to the Λ–type doubling since the splitting is quite small. The calculations of the population rates and transition probabilities however, do require that the two sub–states be considered. This is due to the fact that each component of a Λ–doubled state must be individually populated. Thus, the transition from each upper Λ–doubled state constitutes a fully resolved line.

The volume emission rate of a single molecular line can be expressed as the product of the fractional population of the upper state times a coefficient for spontaneous emission between the two states. For Hund's case (b) transitions, this relationship is given by:

$$E(n'v'N'J'p',n''v''N''J''P'') = N(n'v'N'J'p')\ A(n'v'N'J'p',n''v''N''J''p''), \tag{3–16}$$

where E is the volume emission, N is the fractional population, and A is the Einstein coefficient for the spontaneous emission between the two states. This same relationship holds for the Hund's case (a) states with the only difference being in the parameters that describe the states. Again recall that the single prime refers to the upper state and the double prime refers to the lower state.

The following notation is used for the molecular populations:

N	Total number of molecules
N(n)	Number in electronic state n

$N(nv)$	Number in vibrational level v
Hund's case (a)	
$N(nv\Sigma)$	Number in sub–state Σ
$N(nv\Sigma J)$	Number in rotational level J
$N(nv\Sigma Jp)$	Number with specified parity (+ or –)
Hund's case (b)	
$N(nvN)$	Number in rotational level N
$N(nvNJ)$	Number in rotational level J
$N(nvNJp)$	Number with specified parity (+ or –)

The number of molecules in a specific level described by n' and v' is then denoted $N(n'v')$. In the steady state, this number is given by the productions to the state divided by the losses from the state. The production, or excitation to the energy level is given by $P(n'v')$ and the losses (neglecting collisional quenching) is then given by $\sum_{v''} A_{v'v''}$. This relation is then:

$$N(n'v') = \frac{P(n'v')}{\sum_{v''} A_{v'v''}} . \tag{3–17}$$

Using this relation and multiplying Equation (3–16) by $N(n'v')/N(n'v')$ then gives:

$$E(n'v'N'J'p',n''v''N''J''p'') = P(n'v') \, \frac{N(n'v'N'J'p')}{N(n'v')} \, \frac{A_{J'J''}}{\sum_{v''} A_{v'v''}} , \tag{3–18}$$

where $A_{J'J''}$ is a shortened version for describing the Einstein coefficient A(n'v'N'J'p',n"v"N"J"p").

The production mechanism leading to the emission rate P(n'v') for nitric oxide is photoexcitation. This production rate is proportional to the solar flux and the effective cross section for the transitions to the specific electronic state. The assumption here is that the upper state rotational population distribution is statistically similar to that of the ground state. The branching ratio into the various vibrational levels within the electronic state are given by the Frank–Condon factors. Thus, the population rate can be written:

$$P(n'v') = \pi f \frac{\pi e^2}{mc^2} \lambda^2_{ov'} f_{xn'} q_{ov'} , \tag{3–19}$$

where πf is the solar flux (photons/cm^2/sec/Å), λ is the wavelength of the incoming radiation, $f_{xn'}$ is the oscillator strength for the electronic transition from the ground state to state n', and $q_{ov'}$ is the Frank–Condon factor between the v=0 level of the ground state and the v' level of the upper (n') state. It is assumed here that the molecules initially absorbing the incident radiation are all in the ground state (i.e., v=0 and n=1).

Tatum (1967) gives a detailed description of the calculation determining the relative populations of the molecular energy levels. An overview of that paper is presented here noting the appropriate applications to the nitric oxide bands of interest.

To a very good approximation the fractional population of a given molecular state obeys a Boltzmann distribution which can be expressed as:

$$\frac{N_i}{N} = \frac{g_i e^{-E_i/kT}}{\sum\limits_j g_j e^{-E_j/kT}} , \qquad (3–20)$$

where g_i is the statistical weight of the i^{th} group and the denominator is the associated partition function.

Applying this distribution to the molecular sub–states (Tatum, 1967) gives different results depending upon the type of Hund's coupling to which the state most closely adheres.

For Hund's case (b) and for $\Lambda \neq 0$ the following population relations are given:

$$\frac{N(nvN)}{N(nv)} = \frac{hc\ B_v}{kT}(2N + 1)\exp\left[\frac{hc}{kT}F(N)\right] , \qquad (3–21)$$

$$\frac{N(nvNJ)}{N(nvN)} = \frac{(2J + 1)}{(2S + 1)(2N + 1)} , \qquad (3–22)$$

and

$$\frac{N(nvNJp)}{N(nvNJ)} = \varphi , \qquad (3–23)$$

and for Hund's case (b) in Σ states ($\Lambda = 0$) the following relations are given:

$$\frac{N(nvN)}{N(nv)} = 2\varphi \frac{hc\ B_v}{kT} (2N + 1) \exp\left[\frac{hc}{kT} F(N) \right] , \tag{3–24}$$

$$\frac{N(nvNJ)}{N(nvN)} = \frac{(2J + 1)}{(2S + 1)(2N + 1)} , \tag{3–25}$$

and

$$\frac{N(nvNJp)}{N(nvNJ)} = 1 , \tag{3–26}$$

with $\varphi = \frac{1}{2}$ for heteronuclear molecules like nitric oxide.

Similarly, the population relations for Hund's case (a) are given by:

$$\frac{N(nv\Sigma)}{N(nv)} = \exp\left[-\frac{hc}{kT} A\Lambda\Sigma \right] / \sum_{\Sigma=-S}^{+S} \exp\left[-\frac{hc}{kT} A\Lambda\Sigma \right], \tag{3–27}$$

$$\frac{N(nv\Sigma J)}{N(nv\Sigma)} = \frac{hc\ B_v}{kT} (2J + 1) \exp\left[-\frac{hc}{kT} F(J) \right] , \tag{3–28}$$

and

$$\frac{N(nv\Sigma Jp)}{N(nv\Sigma J)} = \varphi , \tag{3–29}$$

where again $\varphi = \frac{1}{2}$ for heteronuclear molecules.

Then for Hund's case (b), multiplying Equations (3–21), (3–22), and (3–23) gives the fractional population desired from Equation (3–18) for states where $\Lambda \neq 0$ and multiplying Equations (3–24), (3–25), and (3–26) gives the result if $\Lambda = 0$. These results are:

$$\frac{N(nvNJp)}{N(nv)} = \frac{hc\ B_v}{kT}\ \varphi\,\frac{(2J\ +\ 1)}{(2S\ +\ 1)}\ \exp\left[\frac{hc}{kT}\ F(N)\right]\ , \tag{3–30}$$

for states with $\Lambda \neq 0$. The result is simply double this value for states with $\Lambda =$ 0 since there is no Λ–doubling.

Similar equations for the fractional populations for Hund's case (a) molecular states can be obtained by combining Equations (3–27), (3–28), and (3–29). Now that the production rate and the fractional populations can be calculated, the remaining task is to find probabilities of transitions between the various available levels.

3. Selection Rules and Transition Probabilities

Transitions between various energy levels of the molecules adhere to *selection rules.* The emissions of interest in this paper consist of electric dipole radiation and typically obey the following selection rules:

$$\Delta J = 0, \pm 1$$

$$\Delta \Lambda = 0, \pm 1$$

$$\Delta S = 0$$

and

$$(+) \leftrightarrow (-).$$

Recall that the earlier discussion of the rotational transitions only allowed for $\Delta J = \pm 1$ where $\Delta J = J' - J''$. In the total combination of electronic, vibrational, and rotational states the $\Delta J = 0$ transition is also allowed. These three possibilities for ΔJ give rise to three *branches.* The P–branch is for $\Delta J = -1$, the R–branch is for $\Delta J = +1$, and the Q–branch is for $\Delta J = 0$. The upper and lower states for the gamma, delta, and epsilon transitions of nitric oxide are all doublet states so each branch occurs four times. Figures 3–6 and 3–7 show the energy level diagrams for the $^2\Sigma \rightarrow {}^2\Pi$ and the $^2\Pi \rightarrow {}^2\Pi$ transitions involved for the three NO bands of interest. The separate branches are labelled and adherence to the selection rules is clearly shown. In Figure 3–7, the (a) refers to Hund's case (a) and the (b) refers to Hund's case (b) states.

Transitions that do not obey the above selection rules are called *forbidden transitions.* Forbidden transitions exhibit magnetic dipole or electric quadrupole radiation and as a result will not be pursued in this paper.

From Equation (3–18) it was shown that the volume emission rate depended upon the transition probability $A_{J'J''}$. The probabilities for the rotational branching between two vibrational levels can be determined by the Honl–London factors which can be found in Earls (1935) for NO gamma and epsilon band transitions and from Erkovich et. al. (1964) for the delta bands. If the line strengths of the transitions with the same J' are added for a given electronic transition the value $2J + 1$ is obtained. Therefore, it is necessary to divide by this factor to obtain the correct branch probability. In general, the Honl–London factors will only give the probability of a rotational branch for a given v'–v" transition. To consider a transition terminating on that specific lower vibrational level it is necessary to multiply by a factor $A_{v'v''}$. Then $A_{J'J''}$ (or A(n'v'N'J'p',n"v"N"J"p")) can be expressed:

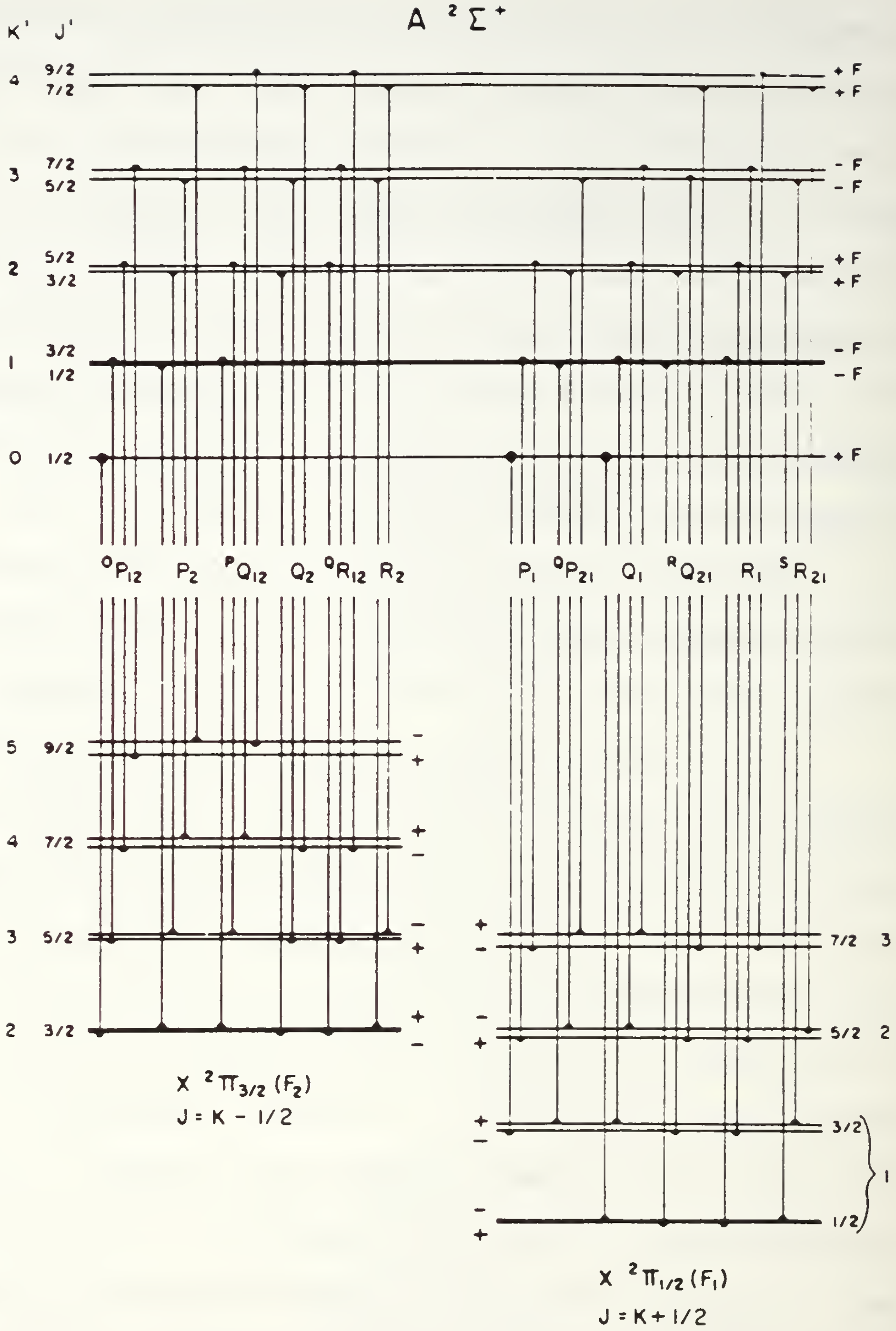

Figure 3–6 Term Diagram for NO Gamma Band Transitions

(from Pearce, 1969)

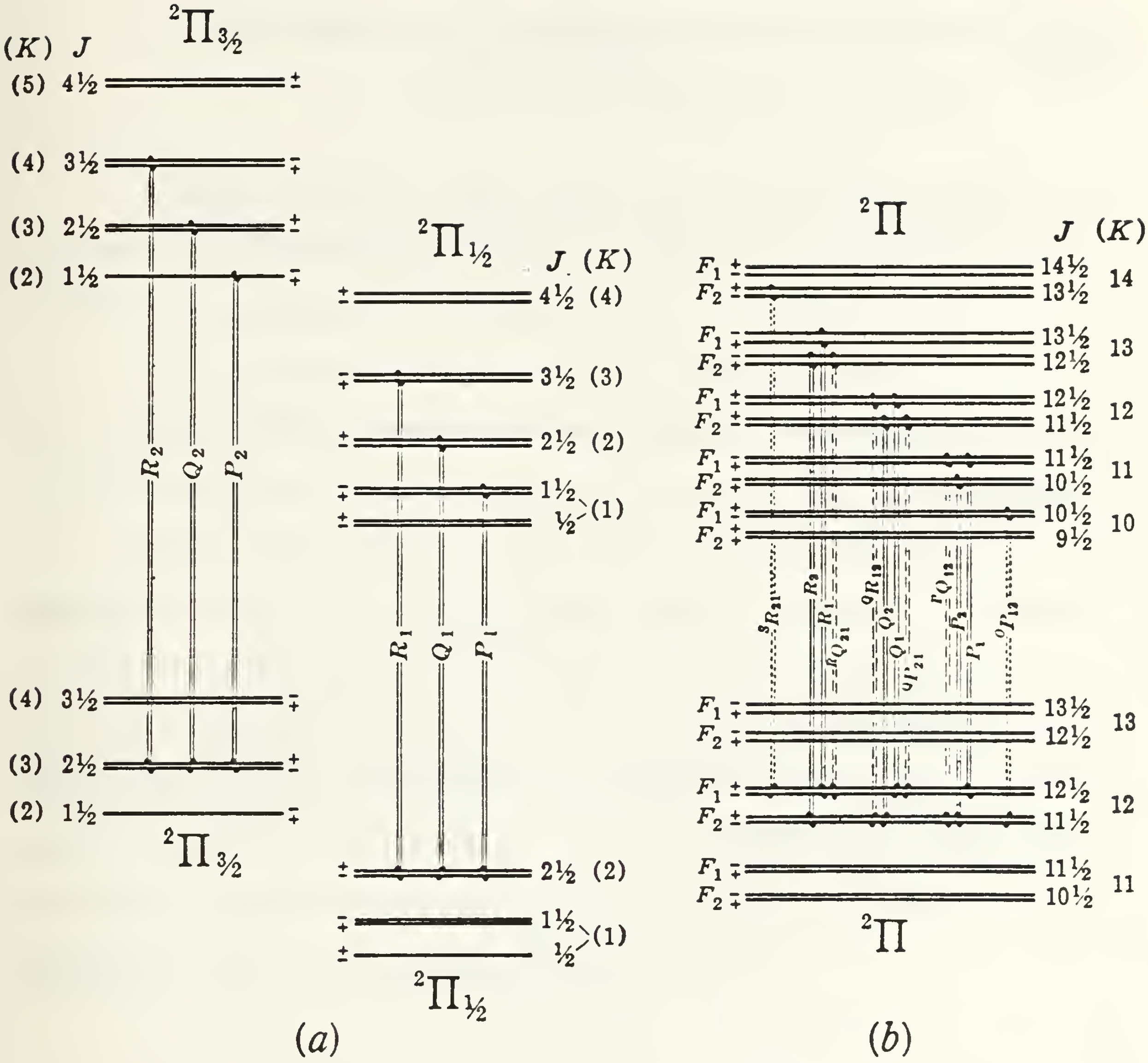

Figure 3–7 Term Diagram for $^2\Pi \rightarrow {}^2\Pi$ Transitions

(from Herzberg, 1950)

$$A(n'v'N'J'p',n''v''N''J''p'') = A_{v'v''} \frac{S(J'J'')}{2J' + 1} , \qquad (3\text{–}31)$$

where S(J'J'') are the tabulated, non–normalized, Honl–London factors.

Equation (3–18) can then be re–written as:

$$E(n'v'N'J'p',n''v''N''J''p'') = \frac{N(n'v'N'J'p')}{N(n'v')} \frac{A_{v'v''}}{\sum\limits_{v''} A_{v'v''}} \frac{S(J'J'')}{2J' + 1} . \qquad (3\text{–}32)$$

The albedo for single–scattering of a fluorescent band (see Barth, 1965) can be expressed as:

$$\tilde{\omega}_{v'v''} = \frac{A_{v'v''}}{\sum\limits_{v''} A_{v'v''}} . \qquad (3\text{–}33)$$

The $A_{v'v''}$ is the transition probability of a molecular band which is related to the band strength by the relation:

$$A_{v'v''} = \frac{64\ \pi^4}{3\ hc^3} \frac{\nu^3_{v'v''}}{d_{v'}} S_{v'v''} , \qquad (3\text{–}34)$$

where $\nu_{v'v''}$ is the frequency of the band, $S_{v'v''}$ is the band strength, and $d_{v'}$ is the degeneracy of the upper level. The band strength, $S_{v'v''}$, can be closely approximated by the product of the electronic transition moment, Re^2, and the associated Frank–Condon factor, $q_{v'v''}$. The albedo for single–scattering can now be given as:

$$\tilde{\omega}_{v'v''} = \frac{\nu^3_{v'v''}}{\sum_{v''} \nu^3 q_{v'v''}} \quad . \tag{3–35}$$

Equations (3–33), (3–34), and (3–35) can be used to get the final expression for the calculation of the volume emission rates from Equation (3–32).

4. Synthetic Spectra Calculations

In the previous sections, the basics of diatomic molecular spectroscopy were introduced and the various elements required for the calculation of the synthetic spectra were presented. The actual calculation of the synthetic spectra for a molecular band requires that the volume emission rate for each line in the band be calculated. The volume emission rates are calculated using Equation (3–32) and the wavelength of the emission is found using Equation (3–5). As each line is determined, its intensity is added to those previously calculated over a given wavelength bin. The process is repeated until the contributions of all of the possible lines have been included. Figure 3–8 is an example of such a synthetically calculated spectrum for the (1,0) gamma band of nitric oxide using a wavelength bin size of 0.03 Å (Cleary, 1985).

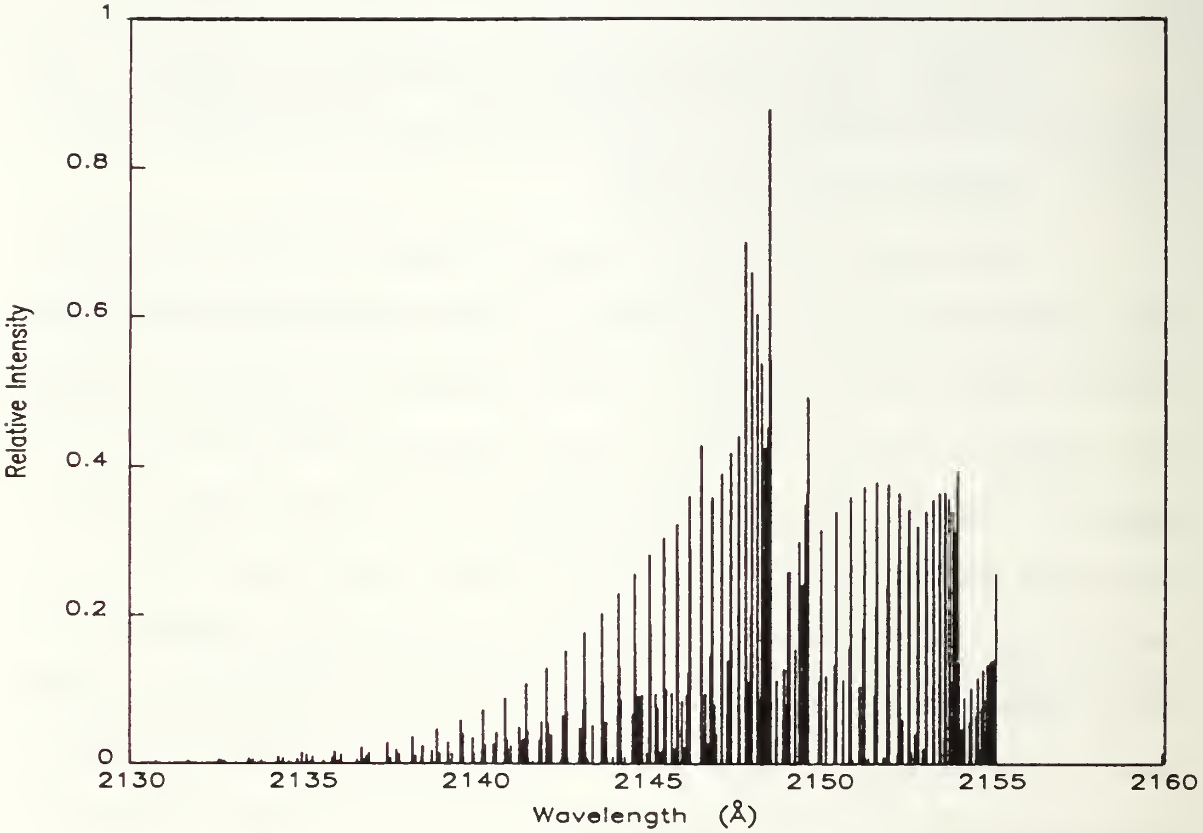

Figure 3–8 Synthetic Spectra for (1,0) Gamma Band Emissions

IV. THE SPACELAB 1 SHUTTLE MISSION

A. INTRODUCTION

The Spacelab 1 shuttle mission was conducted for ten days from November 28 to December 7, 1983. A primary objective of the Spacelab 1 was to obtain an atlas of the dayglow and nightglow emissions over the 300–12700 angstrom range (Torr et. al., 1982; Torr and Torr, 1984). The instrument used for the Spacelab 1 mission was the Imaging Spectrometric Observatory (ISO) and it consisted of five individual spectrometers each designed to operate over a specified portion of the 300–12700 angstrom range. Each of the five individual spectrometers was equipped with its own electronics system that allowed it to be independently controlled. The five spectrometers were located on an instrument pallet in the shuttle cargo bay and the microcomputer system for the control of the instrument was installed inside the Spacelab module.

During the mission, the ISO was operated on 60 different occasions ranging in length from eight minutes to over nine hours. A variety of spacecraft flight attitudes were flown to meet the various requirements of field of view for the instrument.

B. THE INSTRUMENT

The details of the five ISO spectrometers are given in Table 4–1 as reported by Torr et. al. (1982). This paper investigates the data obtained by spectrometer number four (1100 Å – 2300 Å) and to this end the remaining discussion of the instrument design will be limited to that for spectrometer number four.

TABLE 4–1 ISO SPECTROMETER PARAMETER SUMMARY

Spectrometer	Wavelength range (Å)	$\Delta\lambda$ per grating step (Å)	Spectral resolution (Å)	Grating frequency (grooves/mm)	Grating blaze (Å)
1	7500–12000	370	4.5	400	10000
2	4000–8000	326	4.0	450	5500
3	2200–4100	167	2.0	900	3000
4	1100–2300	123	1.5	1200	1500
5	200–1200	123	6.7	1200	800

Table 4–2 contains some additional instrument parameters pertaining specifically to spectrometer number four.

TABLE 4–2 SPECTROMETER NUMBER FOUR PARAMETERS

Photo cathode: CsTe

Grating coating: Al + MgF_2

Focal length: 500 mm

Aperture: 10 X 15 cm^2

Slit length: 5.7 mm

Faceplate window material: MgF_2

Mirror coatings: Al + MgF_2

Mirror type: off–axis parabolic

Field of view: 0.65° X 0.007°

Slit width: 60 μm

The optical design for spectrometer number four is schematically represented in Figure 4–1 (Torr et. al., 1982). Optimum utilization of main and secondary baffle systems as well as low–reflectance surfaces gives an attenuation of approximately 10^{12} against off–axis stray light. For a more detailed description of the ray trace, multiple dispersion, and separation of orders see Torr et. al., (1982).

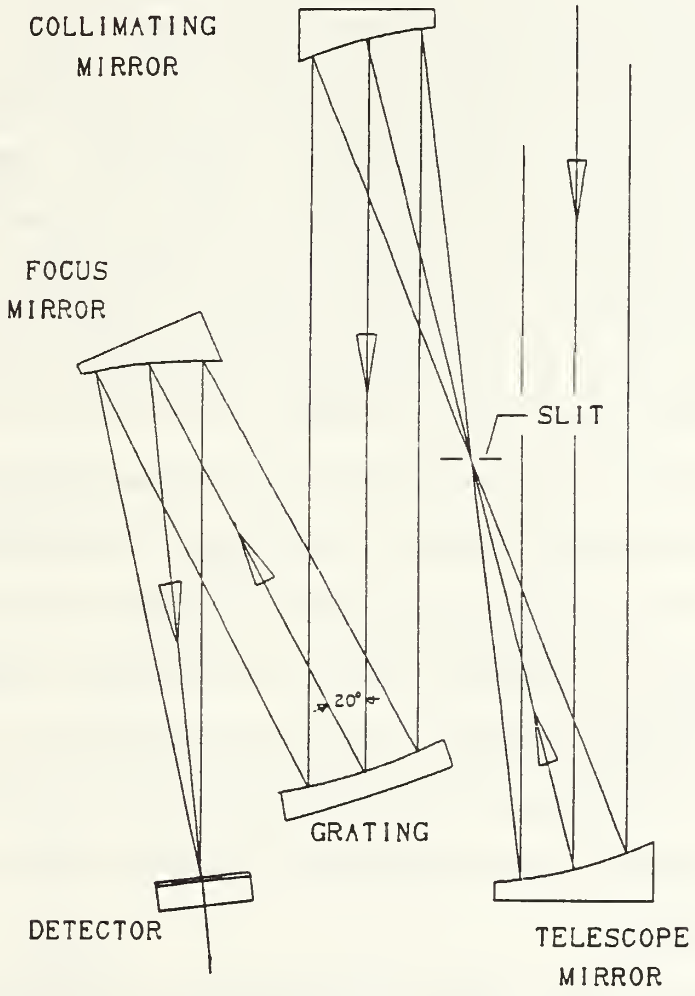

Figure 4–1 Optical Design of Spectrometer

The detector system of the ISO utilizes an intensified two–dimensional charged–coupled device (CCD) array (Torr et. al.,1982; Torr and Torr, 1984). The spectrum is imaged in one dimension while spatial information (corresponding to the length of the entrance slit) is imaged in the other. The CCD consists of 190 X 244 pixels on an active area of silicon that is 5.7 X 4.4 mm. The spectrum is imaged across the 190 pixels and the spatial information is imaged across the 244 pixels.

The components of the detector system include an image intensifier that is aligned with a photocathode at the image plane of the spectrometer. The image intensifier itself contains a semi–transparent photocathode material that is deposited on the window material (faceplate). Both the photocathode material and the window material were selected for the best performance in the desired wavelength range. This in turn is followed by a microchannel plate (MCP) (the primary amplification element) and a phosphor coated fiber–optic bundle. The phosphor has an aluminum coating that limits the resultant photon distribution to 2π steradians in the outgoing direction. Typical gains for such devices range from 3000 to 10000. The use of fiber–optic bundles to couple the photocathode image to the CCD results in negligible loss of output photons generated by the MCP/phosphor coating combination. The noise associated with this system is typically about 60 electrons/pixel/sec. Therefore, two–pixel resolution is achieved for the system. A more complete discussion of the above factors is contained in Torr and Devlin (1982).

The spectrometers were calibrated both spectrally and in absolute intensity prior to the final assembly of the ISO. Spectrometers one through three were calibrated in air while spectrometers four and five were calibrated in a UV vacuum facility (Torr and Vitz, 1982).

C. OVERVIEW

1. Flight Parameters for Low Altitude Viewing

The altitude of the Spacelab 1 shuttle orbit was approximately 250 kilometers. Two methods were used for viewing the atmospheric emissions at altitudes below the spacecraft and each required a special spacecraft flight attitude (Torr and Torr, 1984). In the first method, the instrument entrance slit is aligned to be parallel to the horizon and then the spacecraft is rolled about its nose–tail axis such that the field of view scans downward through the atmosphere. The rate of roll is approximately 0.44 degrees per minute (16° in 36 minutes) and allows for scanning down to a tangent ray height of about 80 kilometers before Rayleigh scattering dominates the signal. Figure 4–2 is a representation of this method.

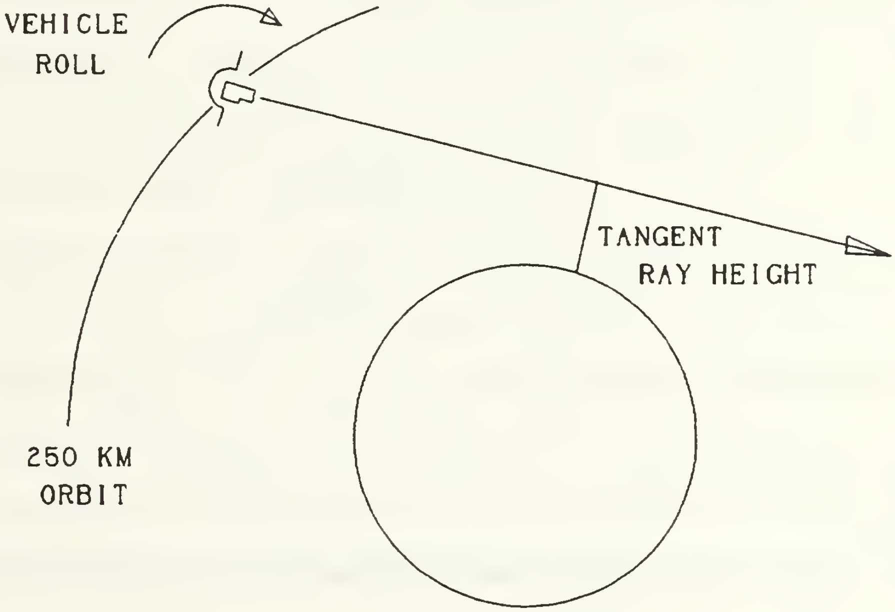

Figure 4–2 Roll Method for Low Altitude Scanning

The second method of viewing takes advantage of the instrument's ability to image spatially along the length of the slit. In this method, the vehicle is positioned such that the entrance slit is perpendicular to the horizon and centered at a particular tangent ray height. Viewing in this manner, approximately 16 kilometers can be resolved simultaneously in two-kilometer increments. It is by this method that the data to be presented in this paper was obtained. Figure 4–3 depicts this method of viewing.

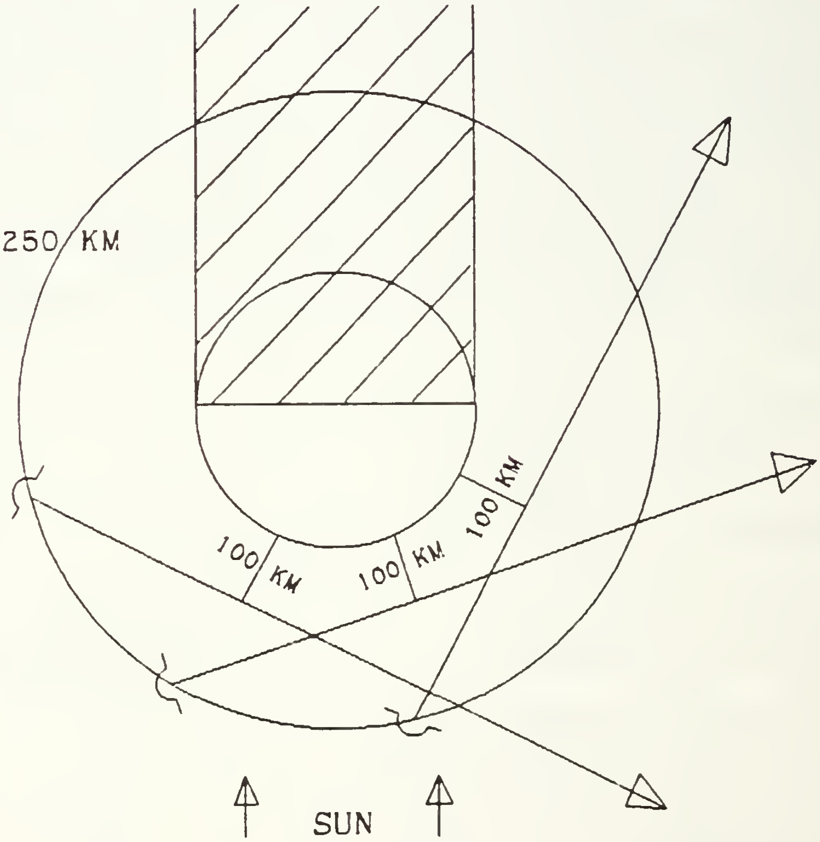

Figure 4–3 Spatial Imaging Method for Low Altitude Viewing

2. The Space Shuttle Optical Environment

It has been observed on the Space Shuttle, as well as on some satellites, that the surfaces directed into the velocity vector tend to develop a bright orange–red glow (Torr et. al., 1977; Yee and Abreu, 1983; Torr, 1983). There is, therefore, concern that optical observations from the Shuttle or other orbiting spacecraft such as the Space Telescope and Space Station may become contaminated or that the measurements may be limited by such glows.

The ISO was designed and mounted into the Shuttle with this situation in mind and as such no surfaces of the Shuttle or payload enter into the field of view of the instrument. Because of this, the instrument was not able to make direct observations of the Shuttle surfaces to gather information on the surface glow. It was decided to extend the mission an extra day and orient the Spacelab such that the z–axis (viewing axis) was pointed directly into the velocity vector. The field of view of the instrument was then tangentially away from the earth at an altitude of approximately 250 kilometers. The orbit of the Spacelab was such that the vehicle was always sunlit but close to the terminator. The solar zenith angle varied between 80 and 100 degrees so the view was of the early morning/late afternoon high–altitude dayglow.

It should be noted that during the assembly of the instrument extreme care was taken to insure that there was no contamination by particulates nor outgassing materials (Torr and Torr, 1985). Once assembled the instrument was kept under clean room conditions and continuous dry nitrogen purge for all phases of spacecraft integration. In light of the fact that every possible precaution within the control and capabilities of the assemblers was taken to prevent contamination, it is believed that the observations made into the velocity vector should include only optical effects of the upper atmosphere and that of the immediate Shuttle environment.

The results of the measurements are discussed by Torr and Torr, 1985 and show that the features one would expect to see in the high–altitude dayglow are indeed present and that the N_2 first positive band system is most likely a predominant factor in the Shuttle glow emmisions. Several possible mechanisms are being investigated to fully understand the effect. (Banks, et. al.,1983; Yee and Abreu, 1983; Green, 1984)

For the purposes of this paper, it is noted that the relative intensities of the emissions in the surface glow are negligible for wavelengths shorter than about 6000 angstroms and as such the effects of the Shuttle glow are not included into the data analysis for the observed spectra between 1800–2300 angstroms.

D. THE OBSERVED SPECTRA

The orbit of the Spacelab 1 Shuttle was between 57°S and 57°N in latitude with an approximate altitude of 250 kilometers. The combination of the high inclination of the orbit and the December time frame resulted in a solar zenith angle that was relatively large so the dayglow observations were of early morning/late afternoon conditions. As previously mentioned, the spectra to be discussed in this paper were obtained utilizing the spatial imaging ability of the ISO.

Marsha Torr of the Marshall Space Flight Center in Huntsville, Alabama is responsible for providing the data files containing the spectra to be analyzed. The seven spectra to be examined in this paper were obtained in two–kilometer altitude increments with the lowest tangent ray height being 96 kilometers and the highest being 108 kilometers.

Other pertinent parameters for the measured spectra include:

- Geographic latitude: 37N
- Geographic longitude: 175E
- Solar zenith angle: 84.8°
- Local time: 16h 07m
- Centering tangent ray height: 103.7 kilometers

Figure 4–4 shows the seven spectra. The lowest spectra corresponds to a tangent ray height of 96 kilometers and the top spectra corresponds to a tangent ray height of 108 kilometers.

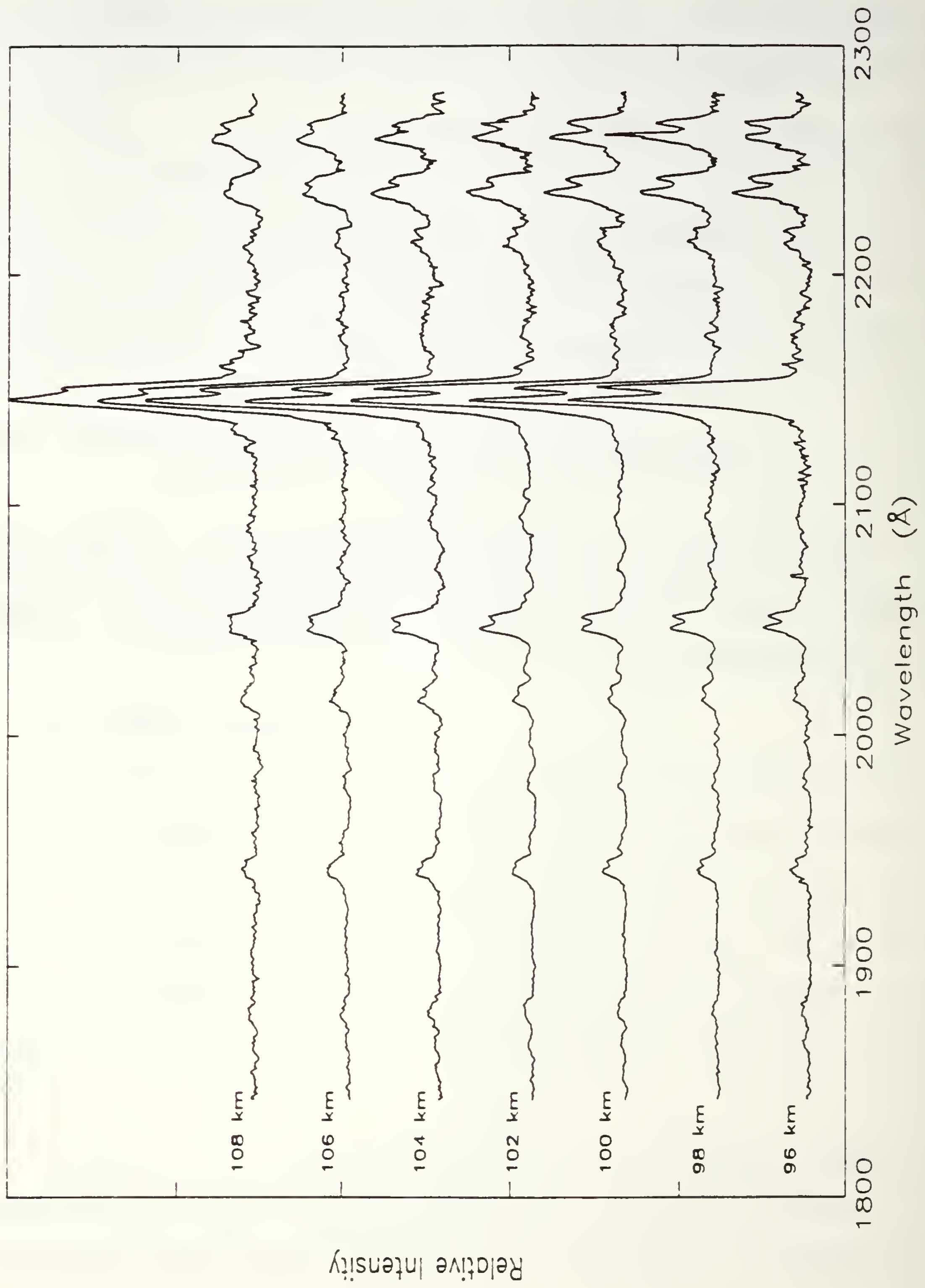

Figure 4–4 Measured Spectra

V. DATA ANALYSIS

A. INTRODUCTION

In this chapter the seven measured spectra from the Spacelab 1 shuttle mission are analyzed by comparison with synthetically generated spectra. The measured spectra cover a wavelength range of approximately 440 angstroms (1840 Å — 2280 Å) in 680 wavelength bins, with each bin covering approximately 0.65 angstroms. The major features of each spectrum are identified and fit by varying 31 of the most prominent emission bands of nitric oxide. The temperature used to obtain the best fits also varied for each spectrum and the results of these temperature variations are compared with the temperature profile as predicted by the MSIS–83 neutral atmosphere model (Hedin, 1983). Variations in the intensities of the major emission features as a function of altitude for the spectra are then discussed and interpretations of these variations are given.

B. APPLICATION OF THE SYNTHETIC SPECTRA

The synthetic spectra calculation discussed in Chapter III can now be accomplished and used to fit the data. Algorithms for the calculation of the nitric oxide γ, δ, and ϵ bands were developed by Cleary (1985). These computer algorithms were checked for correctness by cross referencing the algorithm computational statements to the works of Herzberg, 1950, Pearce, 1969, Earls, 1935, Tatum, 1967, and Barth, 1965. These sources contain calculations and/or predictions for the portions of the synthetic spectra calculation that was presented in Chapter III.

Before the synthetic spectrum was fit to the data it was convolved with the instrument slit function. The slit function was determined self consistently by deconvolving the seven observed spectra with the synthetic spectra. The resulting slit functions were all very similar with each exhibiting a single triangular feature. The slit function obtained from the deconvolution of the 96 km spectrum was chosen as representative since it displayed the least "ringing" outside the central triangle. All of the synthetic spectra discussed below in the fitting process used this instrument slit function whose full width at half maximum was 3.2 Å.

As previously mentioned, nitric oxide emissions dominate the observed portion of the spectrum in this study. However, small contributions due to the Lyman–Birge–Hopfield (LBH) bands and Vegard–Kaplan (VK) bands of molecular nitrogen were also included in the fit which gave additional structure to some of the more minor features. This contribution was quite small and did not hinder the ability to fit the major features with the NO synthetic spectra model.

An additional contribution due to the $N^+(^5S)$ doublet at 2143 Å was considered in the synthetic spectra. This contribution was represented by two delta functions at 2139.68 Å and 2143.55 Å with a relative strength ratio of 48:107 (Cleary and Barth, 1987) respectively. Although the synthetic spectra in the present work underestimates the data in the vicinity of the $N^+(^5S)$ doublet, there was no evidence to suggest that this emission was observed. This is not surprising since, due to collisional quenching, the $N^+(^5S)$ emission is extremely weak at these low altitudes (Bucsela and Sharp, 1989; Torr and Torr, 1985; Siskind and Barth, 1987).

Figure 5–1 shows the breakdown of the various calculated synthetic spectra contributions for the NO gamma, delta, and epsilon bands. Figure 5–2 gives a representative summation and convolution of all the synthetic contributions including the LBH and VK bands.

Due to the 250 kilometer orbit of the shuttle, the line–of–sight path of the spectrometer passes through the higher altitude, higher temperature portions of the atmosphere for low altitude viewing. Therefore, the possibility of contributions to the observed spectra from these higher altitude portions exists. This situation was investigated to determine whether these higher altitude contributions were indeed significant. A model was developed in which the atmosphere was layered into ten, ten–kilometer shells between 100 and 200 km altitude. Each shell was given a temperature based upon the MSIS–83 model and a nitric oxide density based upon a simple scale height model with a density at 100 km of 3 X 10^7 cm^{-3}. Because of the spherical symmetry of the model, the integration path length becomes shorter for each successive higher altitude shell as the observation zenith angle decreases. This factor coupled with lower constituent densities as the altitude increases, quickly degrades any significant contribution to the spectra from the higher altitude segments. Figure 5–3 shows the results of this type of calculation for the gamma (1,0) band emission of nitric oxide which is the most intense emission in the data. As can be seen, the higher temperature contributions tend to broaden the emission band structure as the higher order rotational levels become more populated. This contribution, however, is quite small and therefore its effect will be neglected. Thus, the temperature used to obtain the best fit at a given tangent ray height will be interpreted as the temperature at that altitude.

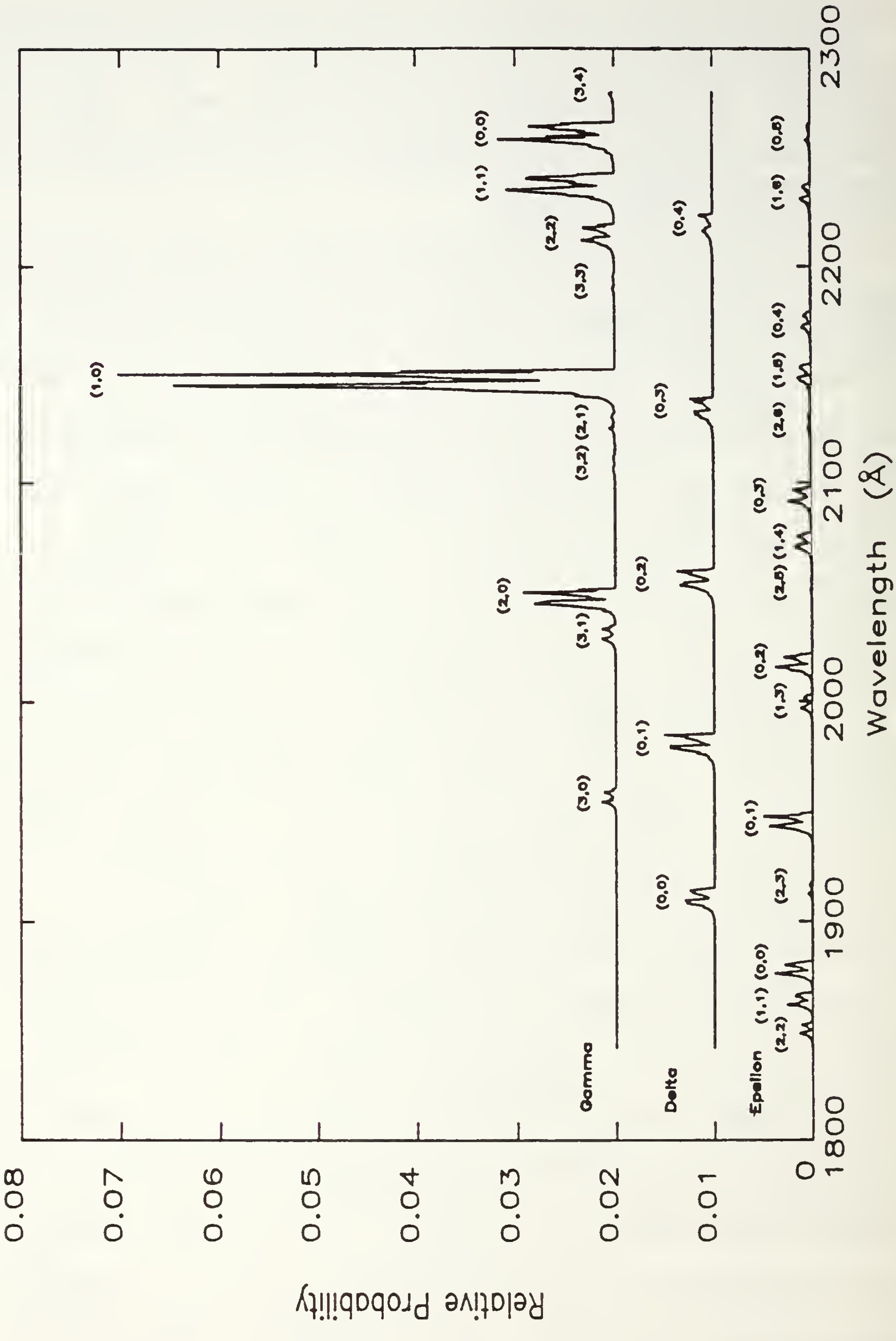

Figure 5–1 Calculated NO Synthetic Spectra

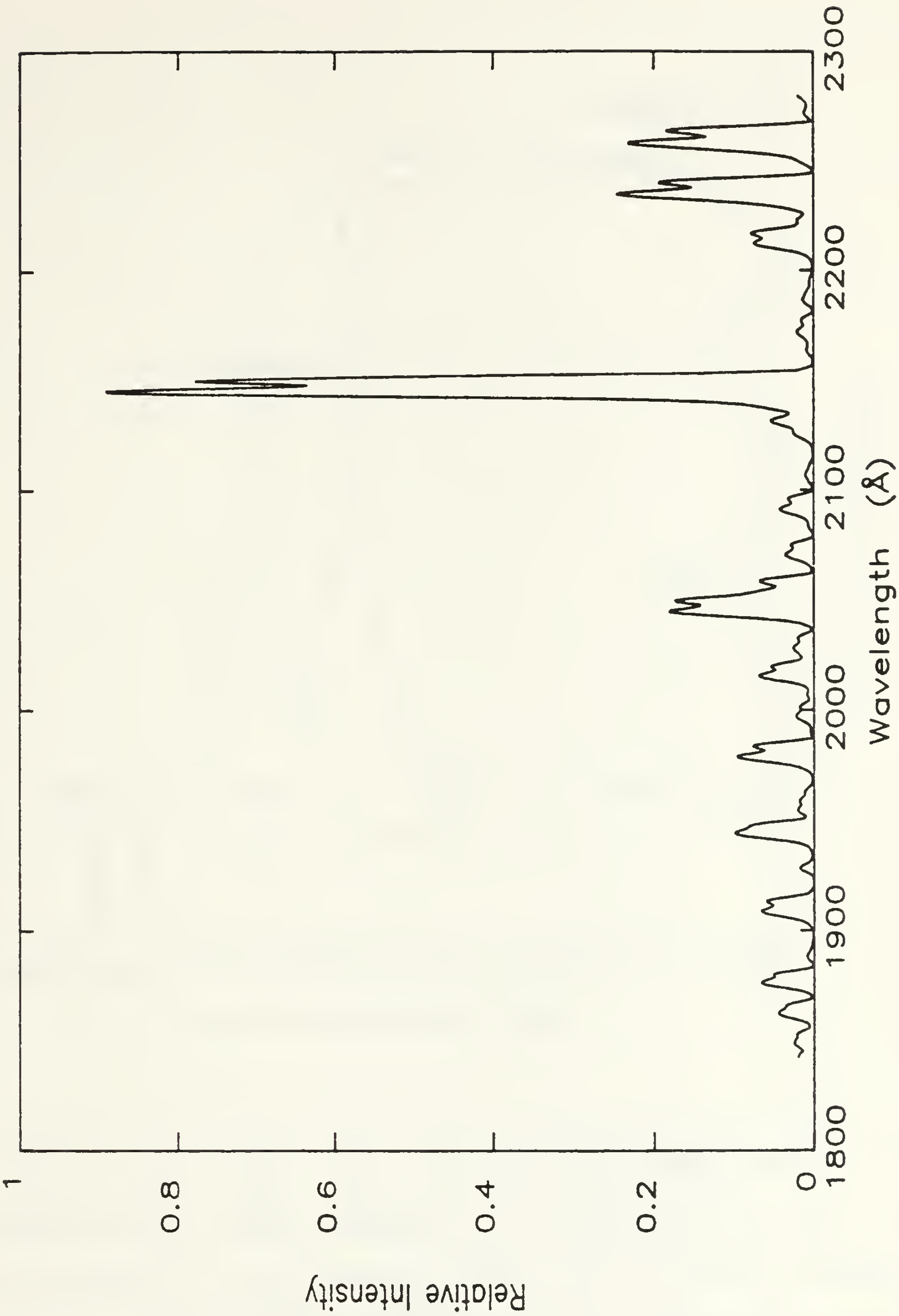

Figure 5–2 Representative Convolved Synthetic Spectrum

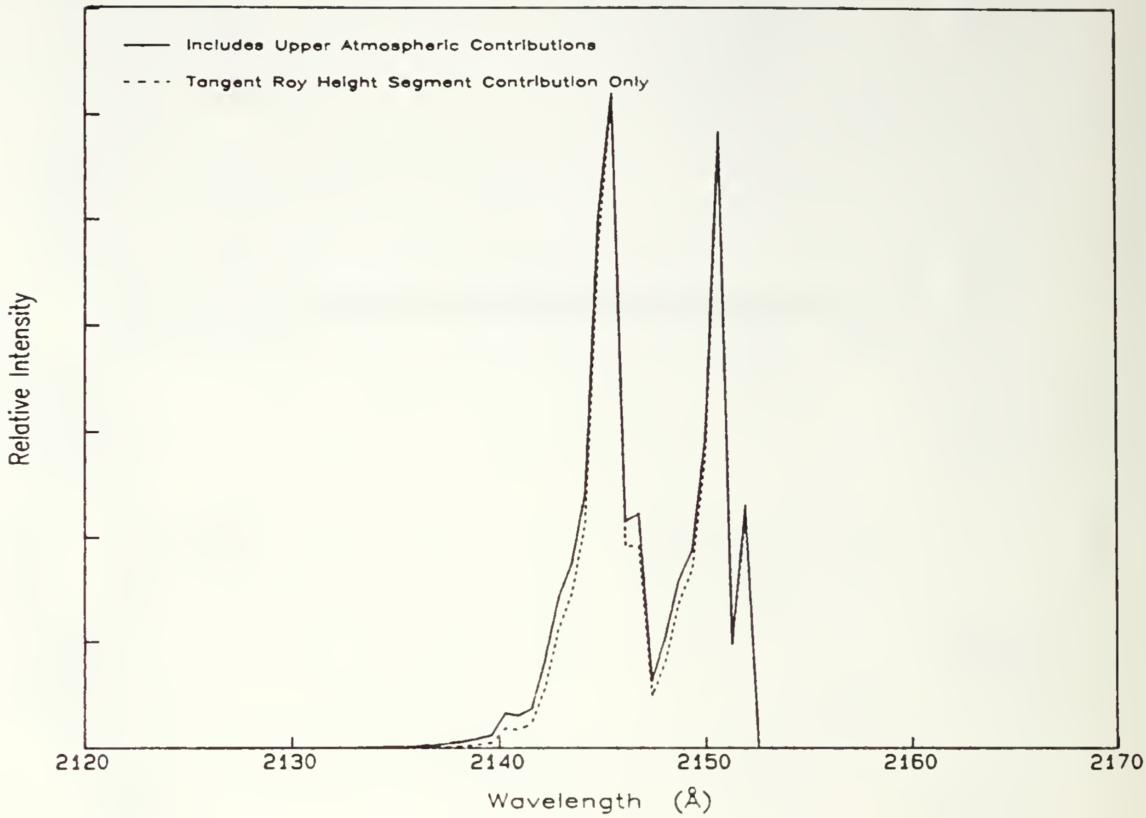

Figure 5–3 Comparison of Synthetic Spectra With and Without Higher Altitude Contributions

C. FITTING THE DATA

As previously mentioned, the measured spectra were fit to the synthetic spectra by varying 31 of the most prominent NO γ, δ, and ϵ band emissions. Figures 5–4 through 5–10 show these results. The tangent ray height in Figure 5–4 is 96 kilometers and increases by two kilometers in each successive figure up to a value of 108 kilometers in Figure 5–10.

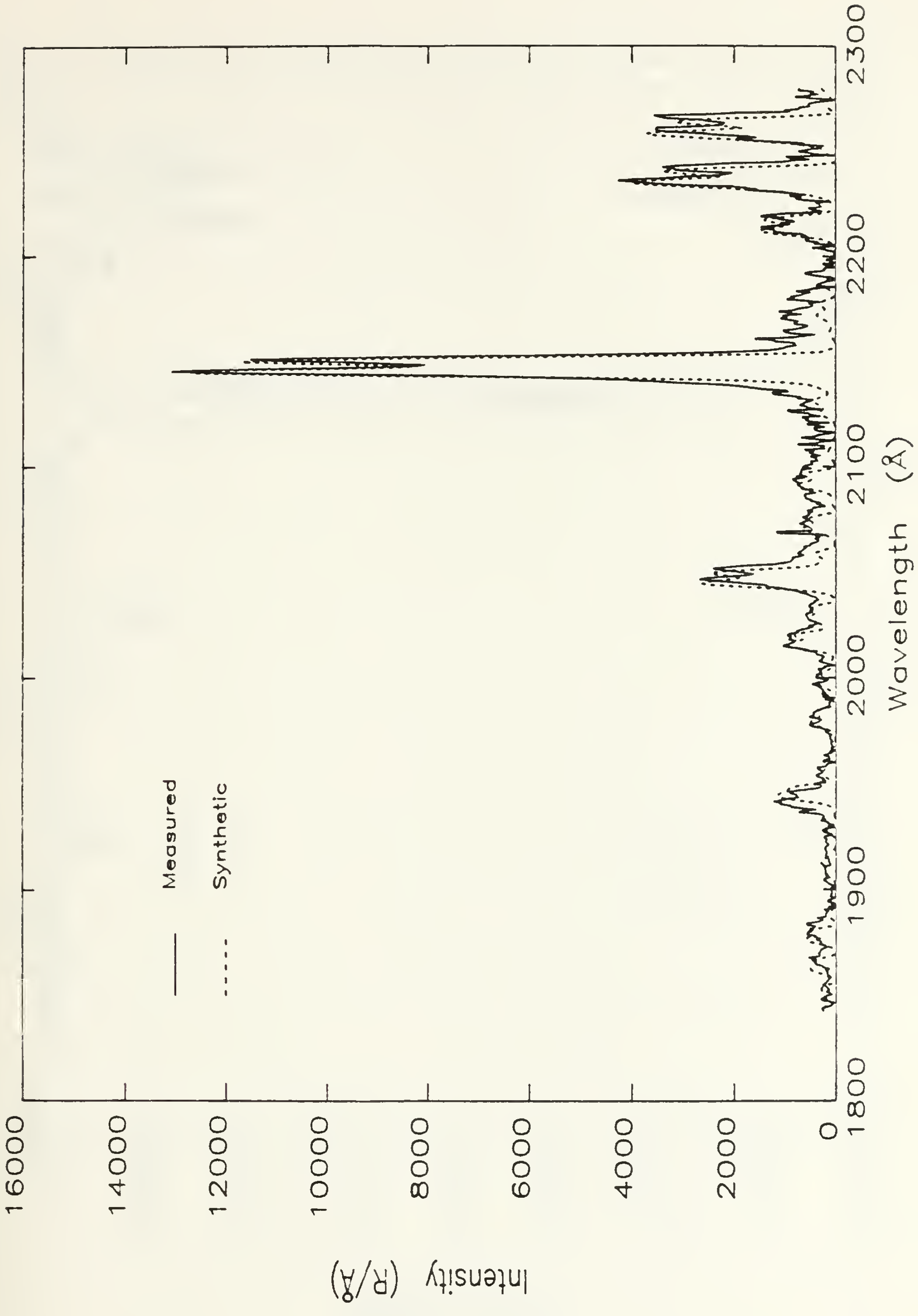

Figure 5–4 Comparison of Data and Synthetic Fit at 96 km

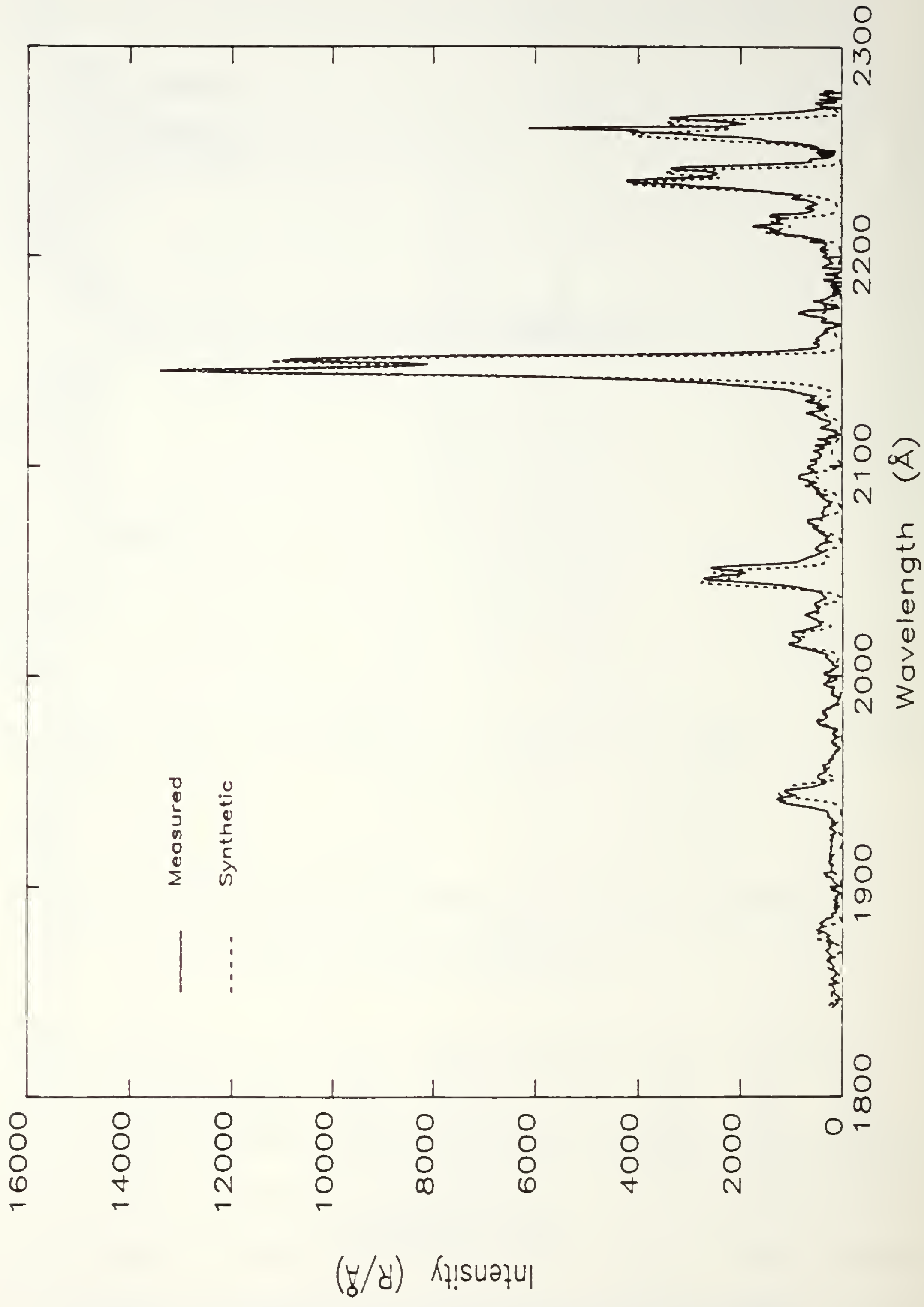

Figure 5–5 Comparison of Data and Synthetic Fit at 98 km

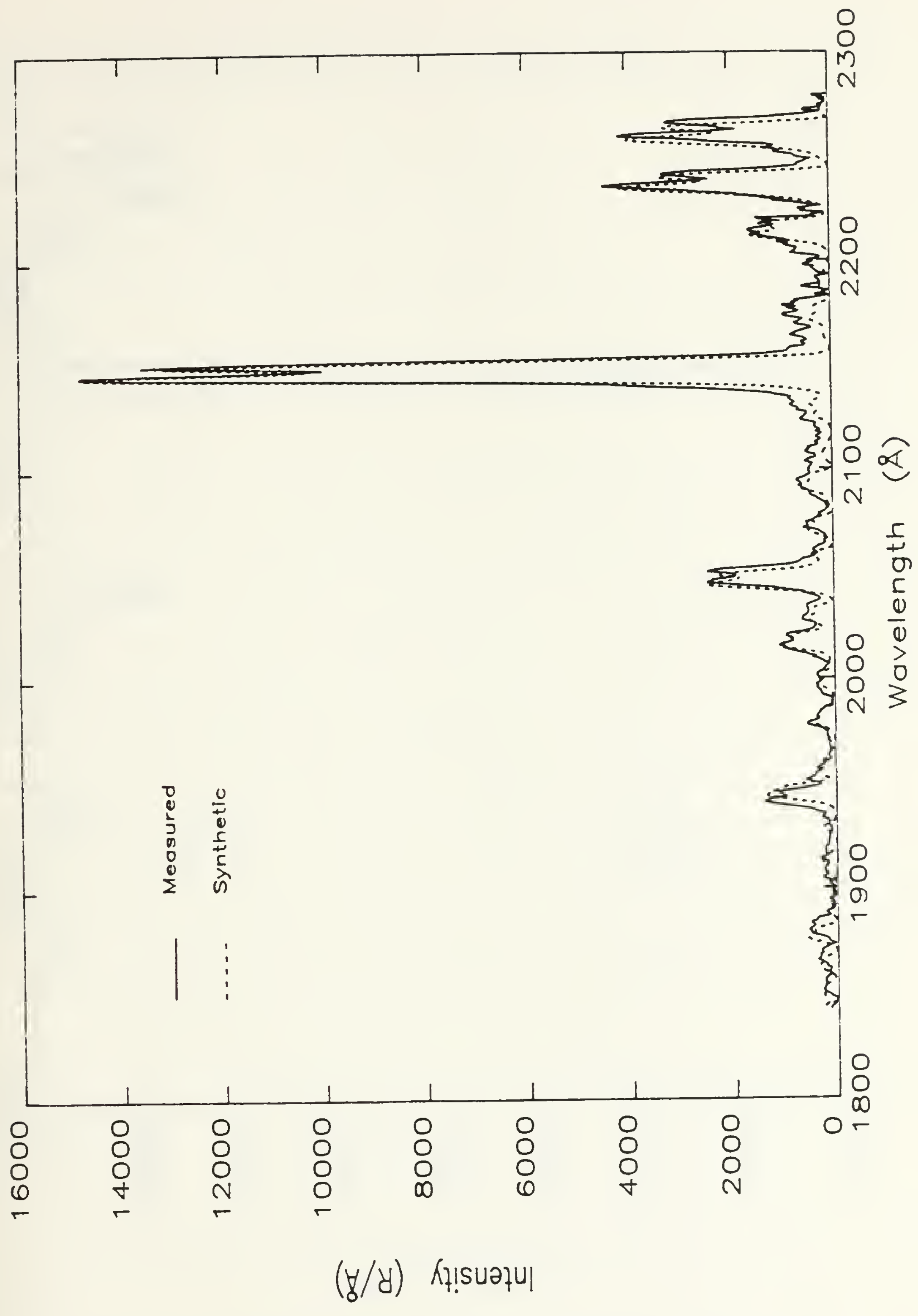

Figure 5–6 Comparison of Data and Synthetic Fit at 100 km

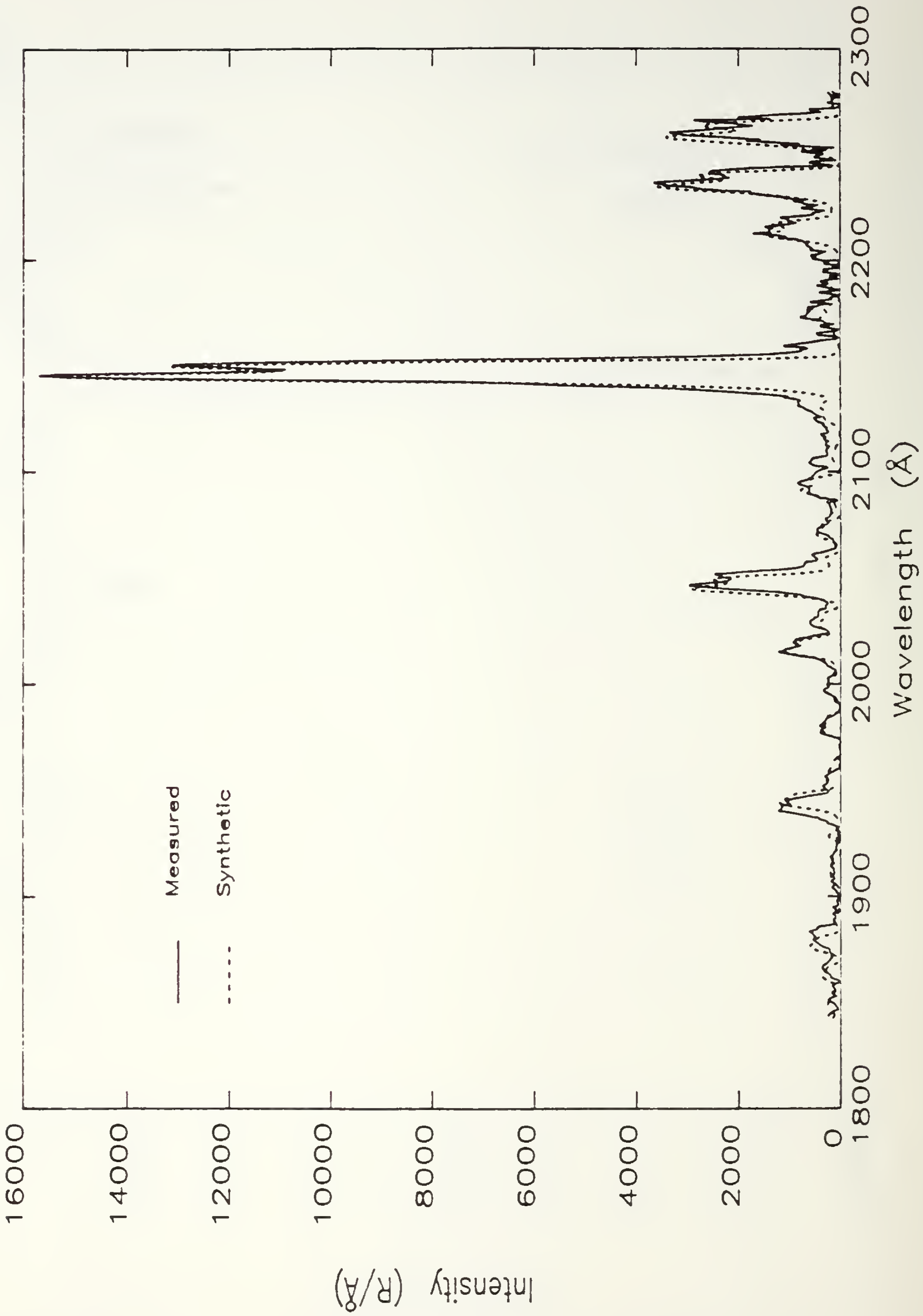

Figure 5–7 Comparison of Data and Synthetic Fit at 102 km

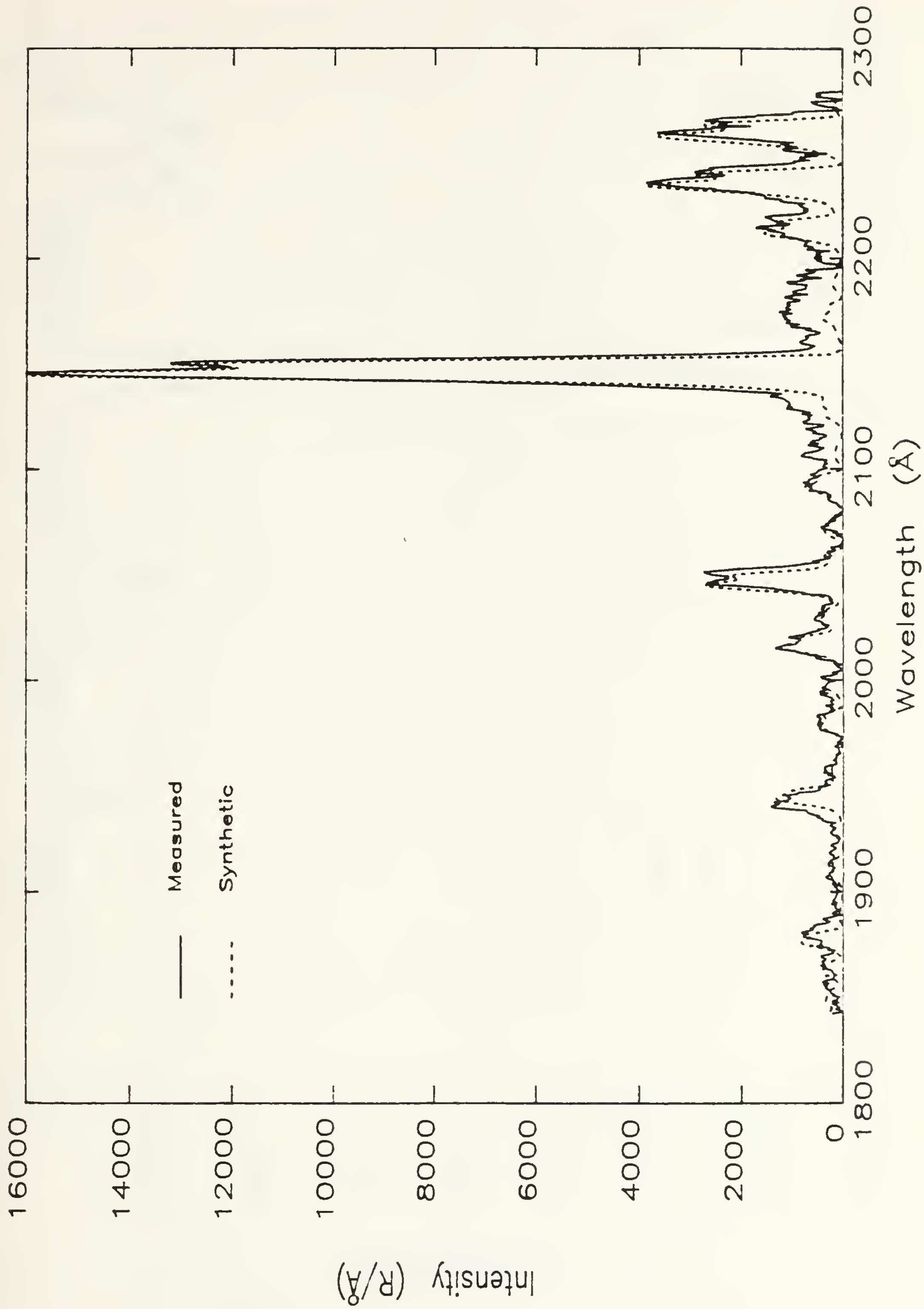

Figure 5–8 Comparison of Data and Synthetic Fit at 104 km

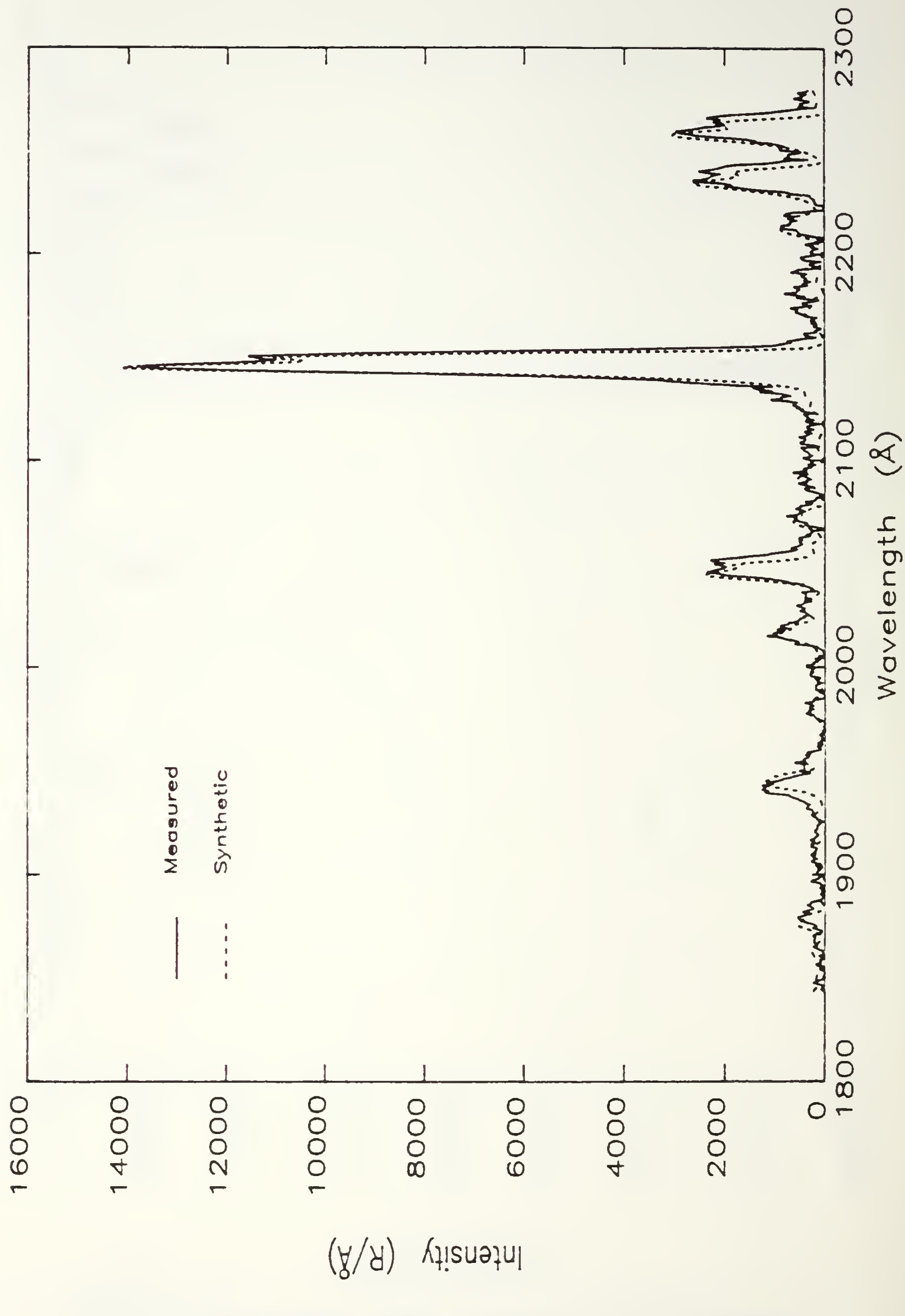

Figure 5–9 Comparison of Data and Synthetic Fit at 106 km

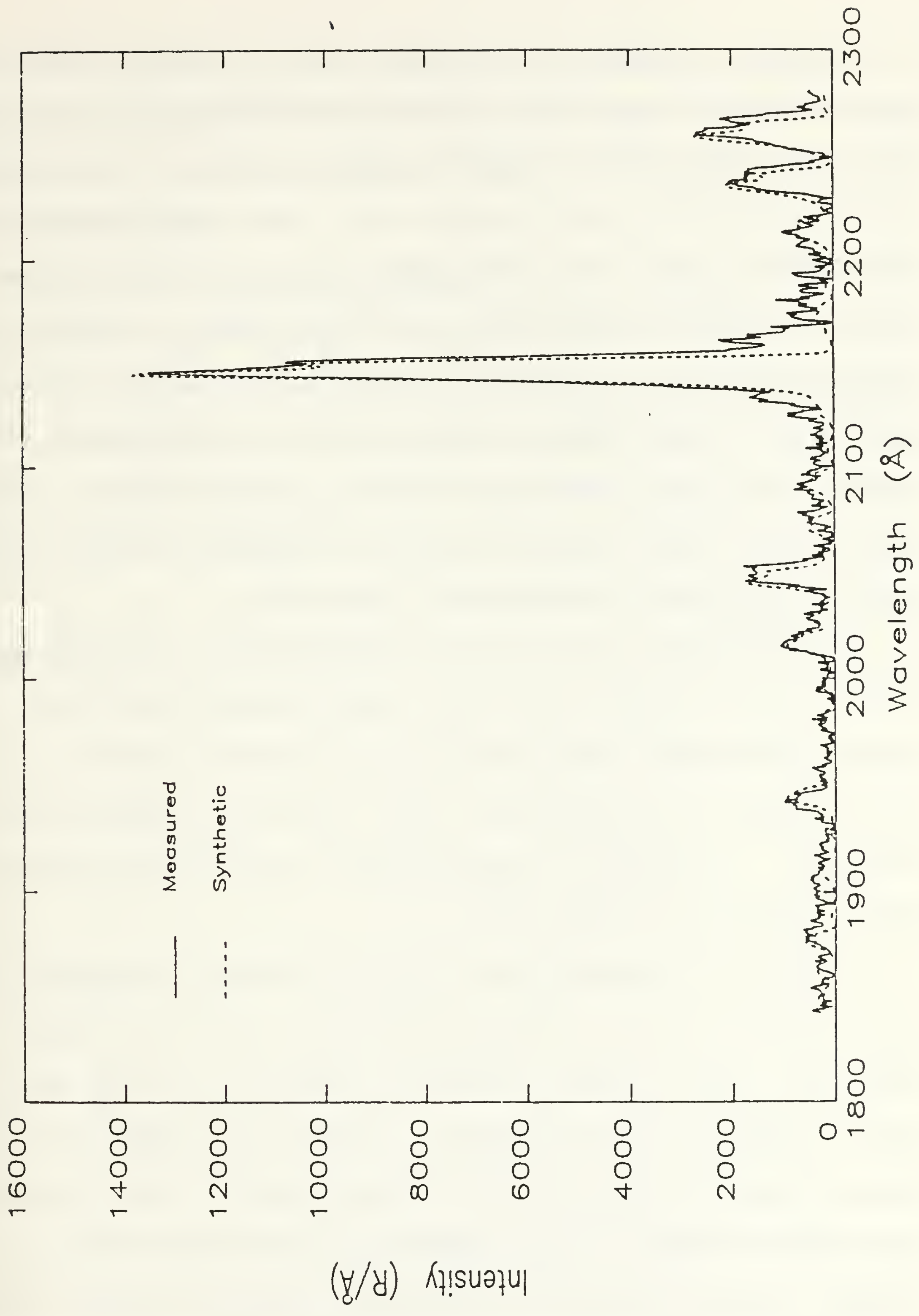

Figure 5–10 Comparison of Data and Synthetic Fit at 108 km

Figures 5–4 through 5–10 show that overall the model is in very good agreement with the measured data. The double bandhead feature is clearly visible in all of the strong emissions of the data which is a result of the branching into the $X^2\Pi_{3/2}$ and $X^2\Pi_{1/2}$ states (see Figure 3–6). Owing to the high resolution of the instrument, many of the minor emission features that would normally be obscured or washed out due to overlap can be clearly observed in the data. For example, the $\epsilon(0,0)$, $\epsilon(1,1)$, and $\epsilon(2,2)$ emissions at 1876 Å, 1862 Å, and 1849 Å respectively can be identified in all of the spectra and are particularly clear in Figure 5–6 which was measured at a tangent ray height of 100 km. Emission intensities that were more than two orders of magnitude smaller than the brightest emissions were identified and fit by the model.

It can also be seen that there are some slight shifts in wavelength between the data and the model in certain areas. These discrepancies are believed to be caused by bin overlaps when the data files were compiled. The entire spectrum was not imaged simultaneously but rather was taken in smaller groups of wavelengths. It is possible that some slight errors were made when combining the separate groups into the final spectrum.

A feature of the observed spectra that was not readily accounted for by the model was the structure in the immediate vicinity of the $\gamma(1,0)$ emission. In nearly every spectrum, there was additional structure on both the longer and shorter wavelength sides of this emission. Increasing the intensity of the $\delta(0,3)$ emission improves the fit on the short wavelength side but does not completely account for the measured values. Additionally, an increase in the $\delta(0,3)$ emission intensity would cause the model to overestimate the data for the $\delta(0,1)$ emission. Some contribution by the NII doublet at 2143 Å would also help in this area but as previously discussed, at these altitudes this contribution is believed to be negligible. Only the $\epsilon(0,4)$ and $\epsilon(1,5)$ emissions can make a contribution on the longer wavelength side and their relative strengths are also small based on their Frank–Condon factors.

Each synthetic spectrum once convolved with the instrument function was then multiplied by a scale factor to bring the intensity into agreement with the data. This scale factor corresponds to the line–of–sight column density for NO. Since the relative intensities of 31 separate emissions could be independently controlled during the fitting process, an average column density was determined from the four most prominent gamma band emissions. These were the $\gamma(0,0)$, $\gamma(1,0)$, $\gamma(1,1)$, and $\gamma(2,0)$ emissions. The results of determining the column density in this way are shown in Figure 5–11. These column densities, however,

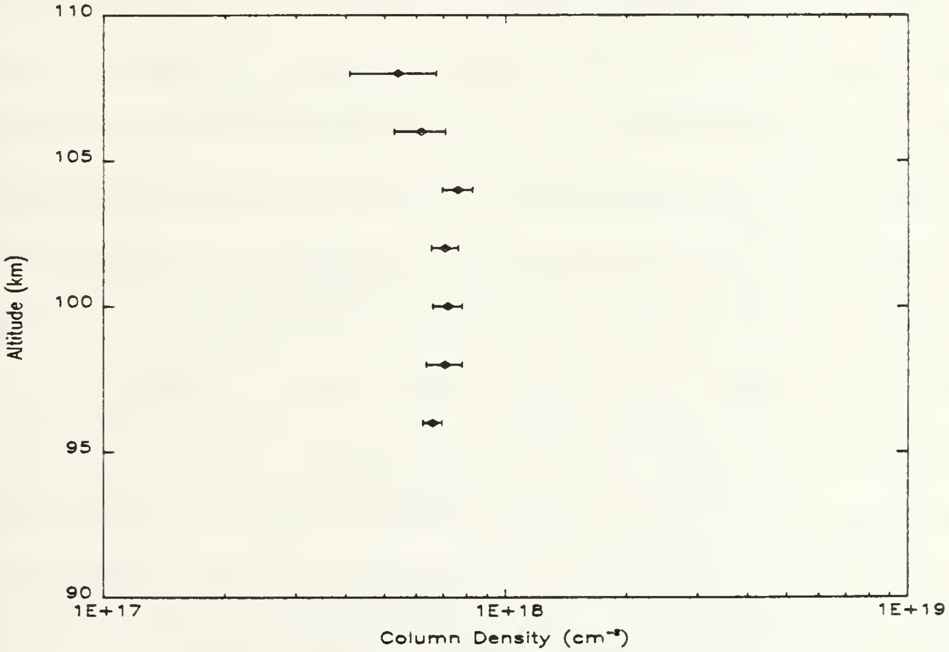

Figure 5–11 NO Column Density

are unusually large. The reason for this discrepancy is believed to be due to an error in the absolute intensity calibration of the instrument. Additional work is required to explain these large observed densities.

D. TEMPERATURE COMPARISON

As each measured spectrum was fit, the temperature used in the calculation of the synthetic spectrum was varied until the best agreement for the match in the double bandhead feature was achieved. As the temperature increases, more rotational states become populated and tend to fill in the double bandhead feature. Recalling Figure 4–4, it is quite apparent how the double bandhead feature begins to fill in as the spectra are taken at higher tangent ray heights, and consequently, higher temperatures. Figure 5–12 shows how varying the temperature can drastically alter the fit of the double bandhead feature of the $\gamma(1,0)$ emission. The middle plot shows the "best" fit and the top and bottom plots show how the fit changes with a 100K temperature variation. By matching this feature the temperature at the tangent ray height could be deduced from the data. Figure 5–13 shows the comparison between the best fit temperatures for each altitude and the temperature profile as computed by the MSIS–83 model. The horizontal error bars reflect the uncertainty in temperature for this fitting procedure. In addition, the single vertical error bar depicts the range of systematic uncertainty based upon the uncertainty in the shuttle orbit altitude and uncertainties in the flight attitude for the viewing angle. That is, the inferred temperatures could be shifted up or down within this range. Both the data and the MSIS–83 model show a strong positive temperature gradient that one expects at these altitudes. The data, however, indicates a stronger temperature gradient than the model reflecting a higher level of solar activity than used by the model.

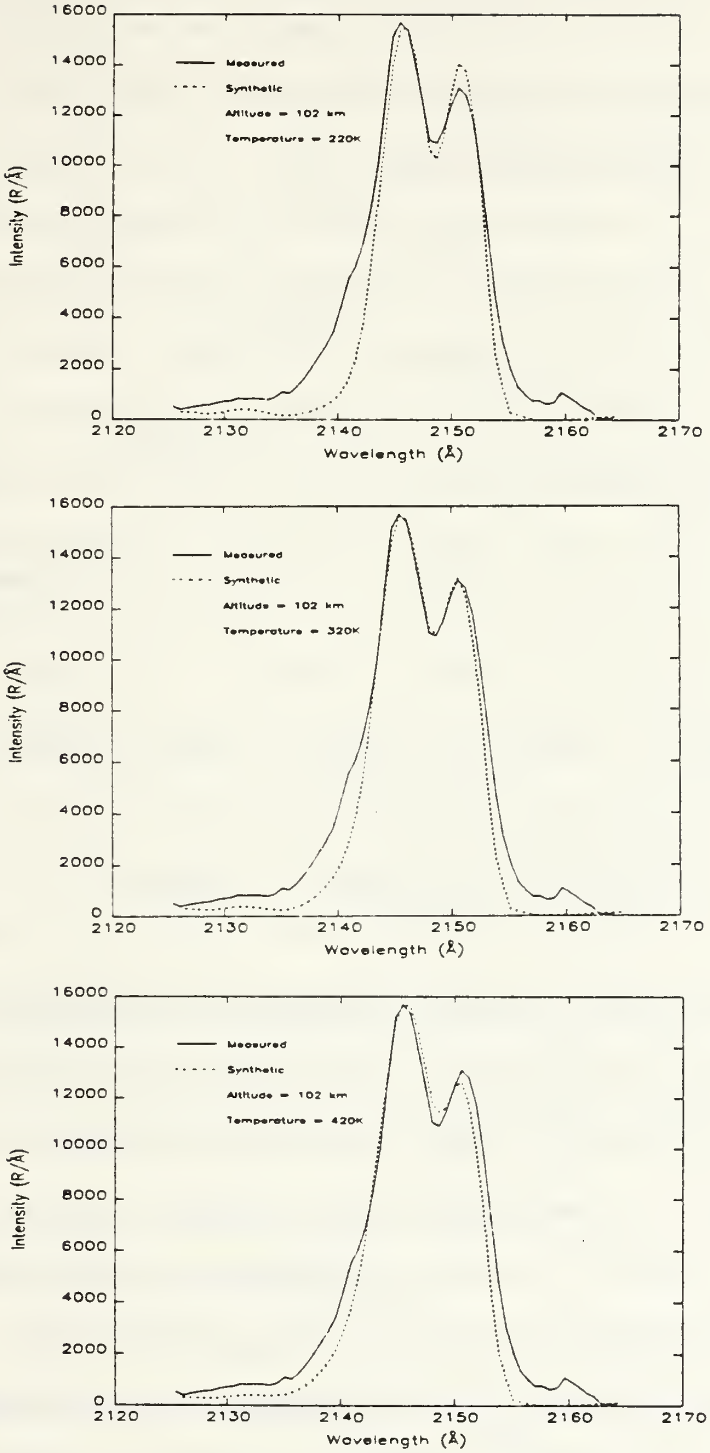

Figure 5–12 Effects of Temperature Variations on the Fit

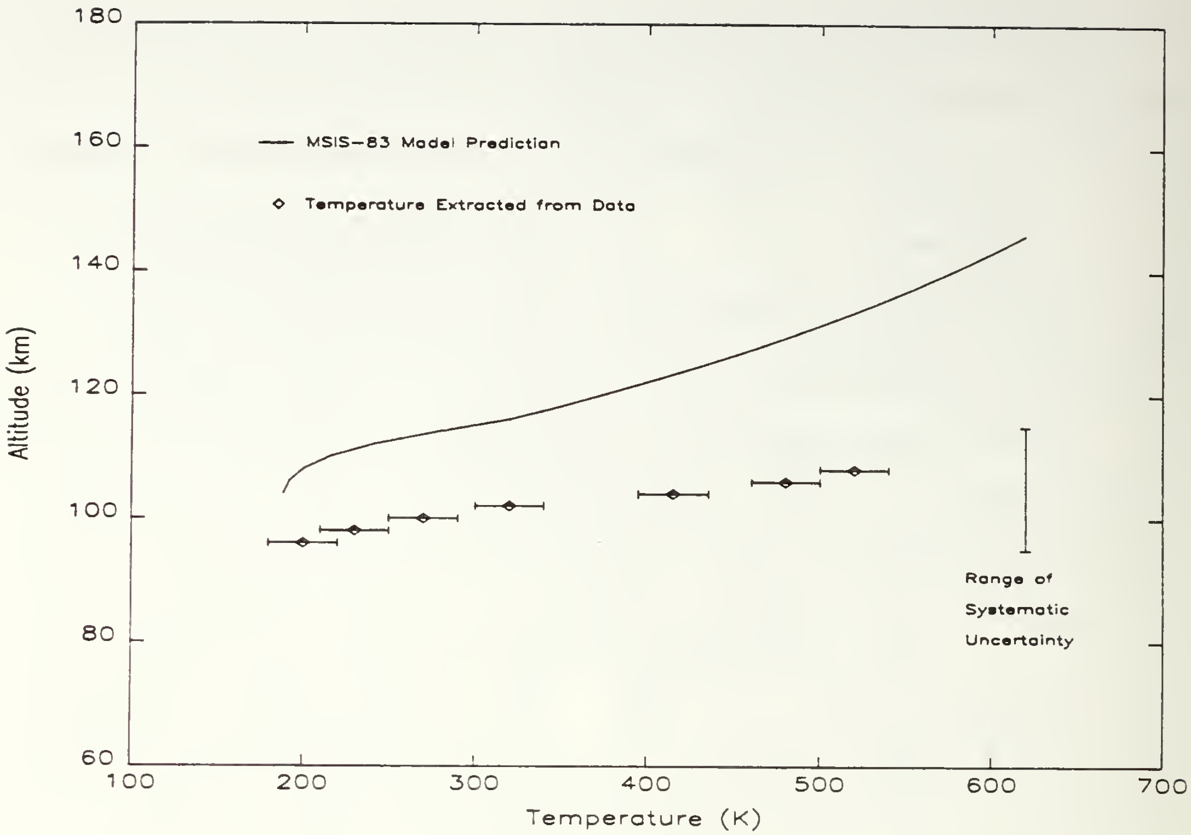

Figure 5–13 Temperature Comparison

E. MEASURED FRANK–CONDON FACTORS FOR THE EPSILON BAND

Individually fitting the emission bands of the data with the synthetic spectra provides a means of verifying the Frank–Condon factors of a given v'' progression. In the data there are four epsilon band emissions that are sufficiently uncontaminated to allow an accurate determination of their Frank–Condon factors. These are the epsilon (0,0), (0,1), (0,2), and (0,3) bands. Since the excitation mechanism is the same for all transitions in a v'' progression, the relative intensities of the emissions within the progression are controlled by the Frank–Condon factors. The column density previously considered can now be used in the determination of these factors. Since the "scale factor" by which each synthetic spectrum was multiplied to fit the data is in fact the column density, a comparison of the column density inferred from the four γ bands (see Figure 5–11) to that calculated by each epsilon band emission of the v" progression is a measure of the correctness of the Frank–Condon factors. The ratios of the γ band NO column density to the ϵ band column densities are shown in Figure 5–14. In the figure the error bars reflect the variations with altitude. These ratios represent corrections for the ϵ band Frank–Condon factors. Had the calculated Frank–Condon factors used in the ϵ band synthetic spectra been correct, the curve in Figure 5–14 would be a straight line with a value of one. In other words, the Frank–Condon factors would have predicted the same NO column density as shown in Figure 5–11. It should be noted that using ratios in this manner eliminates the effect of the uncertainty in the absolute values for the NO column density. Figure 5–15 shows a comparison of the calculated Frank–Condon factors used in the synthetic spectra with those that were determined from the data. The values used in the synthetic spectra calculation are from Spindler et. al., (1970) and Nicholls (1964). The figure suggests stronger weighting of the Frank–Condon factors at higher vibrational levels. It is believed that this is the first experimental determination of the epsilon band Frank–Condon factors.

F. ADDITIONAL FEATURES OF THE SPECTRA

1. Relative Sub–band Intensities

In fitting the measured spectra it was also found that a 20% increase in the intensity for those transitions to the $X^2\Pi_{3/2}$ spin state of NO for the gamma

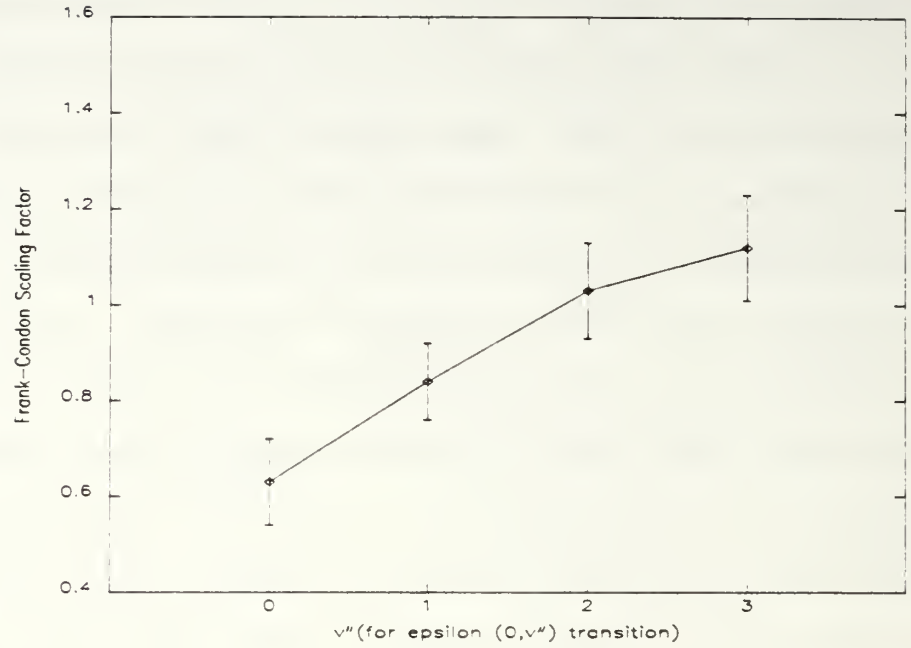

Figure 5–14 v" Progression for v'=0 in Epsilon Band

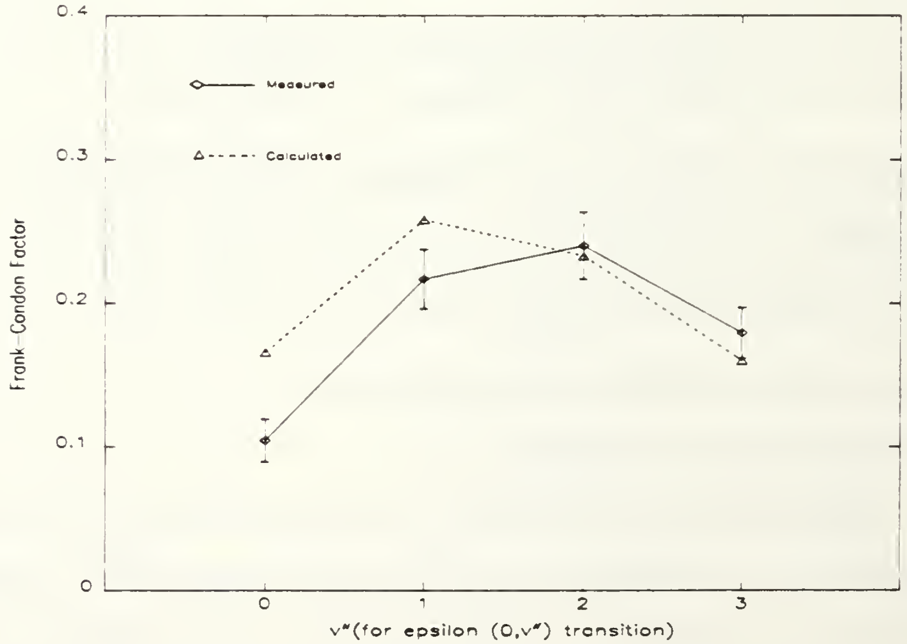

Figure 5–15 Frank–Condon Factor Comparison

and epsilon bands in the synthetic spectra gave much better agreement with the data. The rotational branches requiring the increase are the P_{12}, P_2, Q_{12}, Q_2, R_{12}, and R_2 (recall Figure 3–6). It is believed that the Honl–London factors used in the calculation of these six branches may be in error. The formulae for the calculation of all the Honl–London factors for the gamma and epsilon bands are from Earls, 1935. The reason for this discrepancy is not immediately clear. One possibility as a source of the problem is in the value of the ratio of the molecular state constants A/B as listed in Huber and Herzberg (1979). This ratio enters into the calculation as a measure of the extent of Hund's coupling for the state and could influence the relative strengths of the branches. Figure 5–16 is an example of the fit when this increase is not considered. In nearly every major emission feature it is clear that the longer wavelength side of the emission for the model underestimates the strength of these branches. The final analysis of this situation remains a topic for further investigation. Figures 5–4 through 5–10, however, reflect this increase.

2. NO Delta Bands

Because of predissociation, the fluorescence efficiency of the δ bands has been studied by several aeronomers. This value has been reported to be 0.25 (Cleary, 1986) and 0.2 (McCoy, 1981). The high spectral resolution of the Spacelab 1 spectrometer allowed an excellent fit to the δ (0,1) emission at 1984 Å to be made which resulted in a fluorescence efficiency of 0.32 ± 0.05 when averaged over the seven spectra. This value is consistent with the intensities of the other observed delta bands. In addition, no significant trend with altitude was noted. The fluorescence efficiency obtained in this work, although slightly higher, is in agreement with previously reported results.

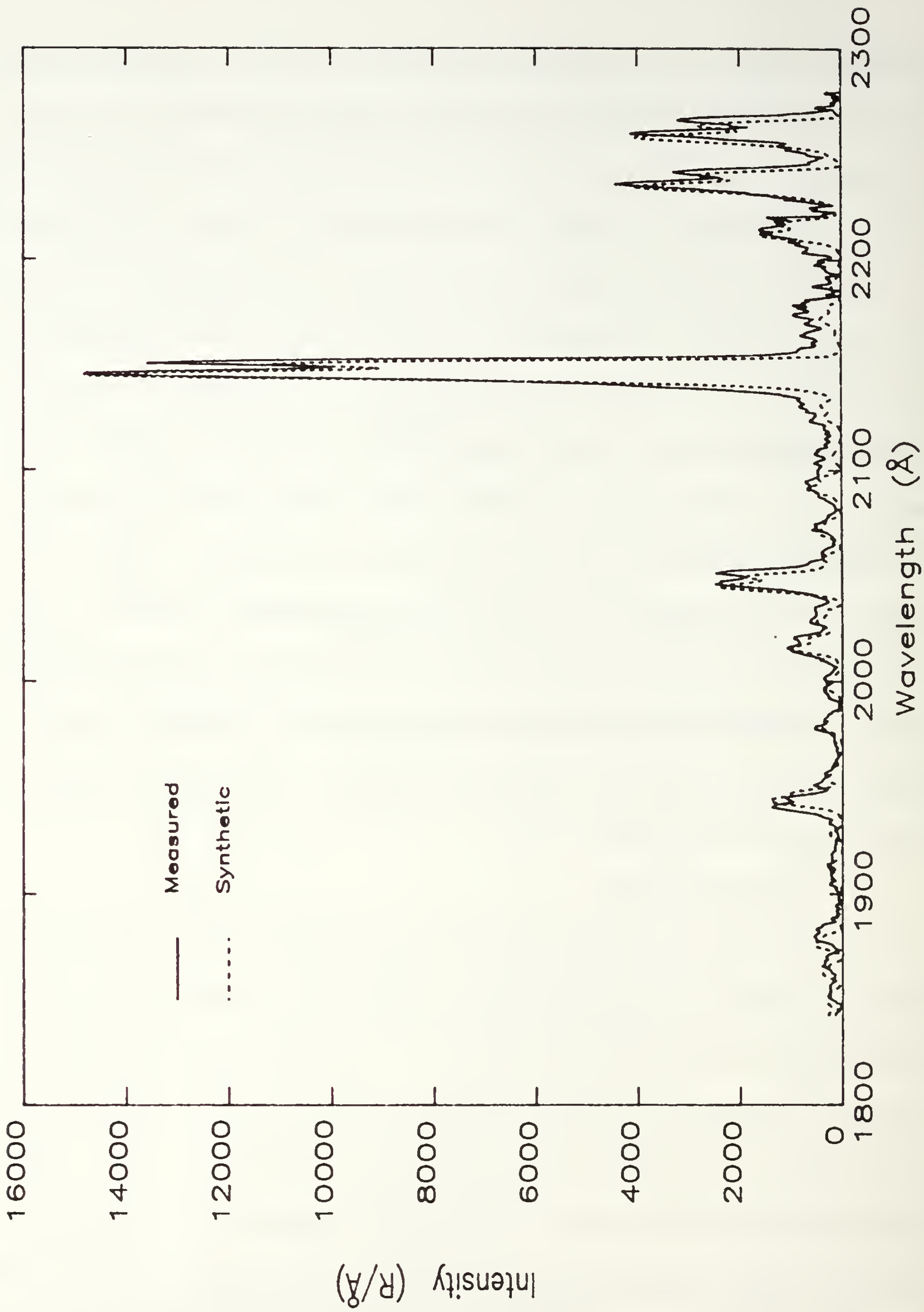

Figure 5–16 Synthetic Fit Without Honl–London Factor Increase

VI. CONCLUSION

A. SUMMARY OF FINDINGS

By fitting the data with the synthetically calculated spectra for the NO gamma, delta, and epsilon band emissions it was possible to identify all of the major features of the measured spectra. The extremely high resolution of the instrument also allowed many of the weaker epsilon band emissions to be clearly identified and gave conclusive evidence of the presence of the epsilon band emissions in the dayglow.

The double bandhead feature of the emissions, due to the $^2\Pi$ ground state of NO, was the key element used in fitting the data. The temperature used in the calculation of the synthetic spectra was varied until this double bandhead feature was best fit (Figure 5–12). The tangent ray height temperatures determined from the data were compared to the temperature profile as predicted by the MSIS–83 model and gave a reasonably similar profile given the range of systematic uncertainty of the tangent ray heights (Figure 5–13). This strong positive temperature gradient as determined from the data is the best evidence that the measured spectra were indeed atmospheric spectra and not simply shuttle glow.

Several trends were noted while fitting the data in various v" progressions. The $\epsilon(0,0)$, $\epsilon(0,1)$, $\epsilon(0,2)$, and $\epsilon(0,3)$ emissions were relatively uncontaminated by other emission features and were thus chosen for a measurement of the Frank–Condon factors. The data suggest that the higher vibrational transitions are weighted more heavily than predicted by the Frank–Condon factors calculated by Nicholls (1964). The inferred Frank–Condon factors are shown in Figure 5–15.

During the course of the data fitting, it was also noted that a 20% increase in the longer wavelength branch Honl–London factors remarkably improved the fit. Figures 5–6 and 5–16 show the comparison of the fits to the data at 100 km with and without the increase. The reason for this discrepancy is not understood but it may be due in part to the values of the molecular constants as tabulated by Huber and Herzberg (1979).

Again owing to the high resolution of the instrument, the delta (0,1) emission was clearly identified and easily fit. By fitting this emission a more accurate estimate of the delta band fluorescence efficiency was obtained. This value was found to be 0.32 ± 0.05 and is slightly higher than the previously reported values by Cleary (1986) and McCoy (1981).

B. TOPICS FOR FURTHER INVESTIGATION

Although this work produced excellent results in several areas, there are some portions of the analysis that require additional study. For example, a further investigation into the Honl–London factor increase for the longer wavelength branches in the gamma and epsilon band emissions is required. In addition, a comparison of observed and calculated Frank–Condon factors for additional v" progressions is needed. Finally, a topic relating specifically to the spectra presented here is a verification of the observed NO column density. The reported value in this paper seems high based upon previously reported values and needs further study.

BIBLIOGRAPHY

Banks, P. M., Williamson, P. R., and Raitt, W. J., "Space Shuttle Glow Observations," *Geophysical Research Letters*, *10*, 118, 1983.

Barth, C. A., "Thermospheric Nitric Oxide and Stratospheric Ozone: Is There a Connection?," *EOS Transactions, American Geophysical Union*, *65*, 1029, 1984.

Bucsela, E. J., and Sharp, W. E., "The Relative Line Strength and Intensity of the NII 2143 Doublet," *Journal of Geophysical Research*, *94*, 12069, 1989.

Cleary, D. D., "Daytime High–Latitude Rocket Observations of the NO γ, δ, and ϵ Bands," *Journal of Geophysical Research*, *91*, 11337, 1986.

Cleary, D. D., and Barth, C. A., "The NII 2143 Å Emission in the Dayglow," *Journal of Geophysical Research*, *92*, 13635, 1987.

Cleary, D. D., *Analysis of Nitric Oxide Fluorescence Bands from High Latitude Rocket Observations of the Thermospheric Dayglow*, Ph.D. Dissertation, University of Colorado, 1985.

Crutzen, P. J., "Ozone Production Rates in an Oxygen–Hydrogen–Nitrogen Atmosphere," *Journal of Geophysical Research*, *76*, 7311, 1971.

Earls, L. T., "Intensities in $^2\Pi$—$^2\Sigma$ Transitions in Diatomic Molecules," *Physical Review*, *48*, 423, 1935.

Eisberg, R., and Resnick, R., *Quantum Physics of Atoms, Molecules, Solids, Nuclei, and Particles*, Second Edition, John Wiley & Sons, Inc., 1985.

Erkovich, S. P., Pisarevskii, Y. V., and Ageshin, F. S., "A Method of Determining Oscillator Strengths for Electronic Transitions in Molecules," *Optical Spectra*, *17*, 15, 1964.

Gilmore, F. R., "Potential Energy Curves for N_2, NO, O_2, and Corresponding Ions," *Journal of Quantitative Spectroscopy and Radiative Transfer*, *5*, 369, 1965.

Green, B. D., "Atomic Recombination into Excited Molecular—A Possible Mechanism for Shuttle Glow," *Geophysical Research Letters*, *11*, 576, 1984.

Hedin, A. E., "A Revised Thermospheric Model Based on Mass Spectrometer and Incoherent Scatter Data: MSIS–83," *Journal of Geophysical Research*, *88*, 10170, 1983.

Herzberg, G., *Molecular Spectra and Molecular Structure I. Spectra of Diatomic Molecules*, D. Van Nostrand Company, Inc., 1950.

Huber, K. P., and Herzberg, G., *Molecular Spectra and Molecular Structure IV. Constants of Diatomic Molecules*, Van Nostrand Reinhold Company, 1979.

Hund, F., "Zur Deutung der Molekulspektren. II," *Zeitschrift Physik*, *42*, 93, 1927.

Ingle, J. D., and Crouch, S. R., *Spectrochemical Analysis*, Prentice Hall, Inc., 1988.

McCoy, R. P., *Rocket Measurements of Thermospheric Odd Nitrogen and Comparisons with a Diffusive Transport Chemical Model*, Ph.D. Dissertation, University of Colorado, 1981.

Mount, G. H., and Rottman, G. J., "The Solar Absolute Spectral Irradiance 1150–3173 Å: 17 May 1982," *Journal of Geophysical Research, 88*, 5403, 1983.

NASA Technical Report 32–822, *Ultraviolet Spectroscopy of Planets*, C. A. Barth, 1965.

Nicholls, R. W., "Frank–Condon Factors to High Vibrational Quantum Numbers IV: NO Band Systems," *Journal of Research of the National Bureau of Standards*, *68A*, No. 5, 1964.

Pearce, J. B., "Nitric Oxide Gamma Band Emission Rate Factor," *Journal of Quantitative Spectroscopy and Radiative Transfer*, *9*, 1593, 1969.

Siskind, D. E., and Barth, C. A., "Rocket Observations of the NII 2143 Å Emission in an Aurora," *Geophysical Research Letters*, *14*, 479, 1987.

Spindler, R. J., Jr., Isaacson, L., and Wentink, T., Jr., "Frank–Condon Factors and R–Centroids for the Gamma System of NO," *Journal of Quantitative Spectroscopy and Radiative Transfer*, *10*, 621, 1970.

Strobel, D. F., Hunten, D. M., and M^{c}Elroy, M. B., "Production and Diffusion of Nitric Oxide," *Journal of Geophysical Research*, *75*, 4307, 1970.

Tascione, T. F., *Introduction to the Space Environment*, Orbit Book Company, Inc., 1988.

Tatum, J. B., "The Interpretation of Intensities in Diatomic Molecular Spectra," *The Astrophysical Journal Supplement Series*, *14*, 21, 1967.

Torr, M. R., Basedow, R. W., and Torr, D. G., "Spectroscopic Imaging of the Thermosphere from the Space Shuttle," *Applied Optics*, *21*, 4130, 1982.

Torr, M. R., Basedow, R. W., and Mount, J., "An Imaging Spectrometric Observatory for Spacelab," *Astrophysics and Space Science*, *92*, 237, 1983.

Torr, M. R., and Torr, D. G., "Atmospheric Spectral Imaging," *Science*, *225*, 169, 1984.

Torr, M. R., and Vitz, R. C., "Extreme Ultraviolet Imaging Spectrometer for Thermospheric Emissions," *Applied Optics*, *21*, 3080, 1982.

Torr, M. R., and Devlin, J., "Intensified Charge Coupled Devices for Use as a Spaceborne Spectrographic Image Plane Detector System," *Applied Optics*, *21*, 3091, 1982.

Torr, M. R., Hays, P. P., Kennedy, B. C., and Walker, J. C. G., "Intercalibration of Airglow Observations with the Atmosphere Explorer Satellite," *Planetary Space Science*, *25*, 173, 1977.

Torr, M. R., "Optical Emissions Induced by Spacecraft–Atmosphere Interactions," *Geophysical Research Letters*, *10*, 114, 1983.

Torr, M. R., and Torr, D. G., "The NII 2143 Å Dayglow from Spacelab 1," *Journal of Geophysical Research*, *90*, 6679, 1985.

Yee, J. H., and Abreu, V. J., "Visible Glow Induced by Spacecraft–Environment Interaction," *Geophysical Research Letters*, *10*, 126, 1983.

INITIAL DISTRIBUTION LIST

1. Defense Technical Information Center 2
Cameron Station
Alexandria, Virginia 22304–6145

2. Library, Code 0142 2
Naval Postgraduate School
Monterey, California 93943–5002

3. Dr. K. E. Woehler, Chairman 1
Physics Department
Naval Postgraduate School
Monterey, California 93943–5000

4. Dr. D. D. Cleary 5
Physics Department, 61–Cl
Naval Postgraduate School
Monterey, California 93943–5000

5. Dr. S. Gnanalingam 1
Physics Department, 61–Gm
Naval Postgraduate School
Monterey, California 93943–5000

6. Dr. M. R. Torr 1
Space Science Laboratory
George C. Marshall Space Flight Center
Marshall Space Flight Center, Alabama 35812

7. Dr. R. McCoy 1
Code 4140
Naval Research Laboratory
Washington D.C. 20375

8. LT James L. Bosserman, USN 1
Naval Ship Weapons Systems Engineering Station
Port Hueneme, California 93043–5007

8/92-583

Thesis
B72636 Bosserman
c.1 Analysis of thermospheric dayglow spectra from the Spacelab 1 shuttle mission.

11 NOV 92

38080

Thesis
B72636 Bosserman
c.1 Analysis of thermospheric dayglow spectra from the Spacelab 1 shuttle mission.

AMERICAN BINDERY
2
TOPEKA KANSAS

Analysis of thermospheric dayglow spectr
3 2768 000 88284 9
DUDLEY KNOX LIBRARY